

## Review

# Gold-based Inorganic Nanohybrids for Nanomedicine Applications

Xianguang Ding<sup>1</sup>, Dan Li<sup>2</sup> and Jiang Jiang<sup>3,4</sup>✉

1. Key Laboratory for Organic Electronics and Information Displays & Jiangsu Key Laboratory for Biosensors, Institute of Advanced Materials (IAM), Nanjing University of Posts and Telecommunications, Nanjing, 210023, China.
2. Department of Dermatology, Nanjing Drum Tower Hospital, The Affiliated Hospital of Nanjing University Medical School, Nanjing, 210008, China.
3. i-Lab and Division of Nanobiomedicine, CAS Key Laboratory of Nano-Bio Interface, CAS Center for Excellence in Nanoscience, Suzhou Institute of Nano-Tech and Nano-Bionics, Chinese Academy of Sciences, Suzhou, 215123, China.
4. School of Nano-Tech and Nano-Bionics, University of Science and Technology of China, Hefei, 230026, China.

✉ Corresponding author: Jiang Jiang, E-mail: [jjiang2010@sinano.ac.cn](mailto:jjiang2010@sinano.ac.cn).© The author(s). This is an open access article distributed under the terms of the Creative Commons Attribution License (<https://creativecommons.org/licenses/by/4.0/>). See <http://ivyspring.com/terms> for full terms and conditions.

Received: 2019.11.19; Accepted: 2020.06.18; Published: 2020.07.02

## Abstract

Noble metal Au nanoparticles have attracted extensive interests in the past decades, due to their size and morphology dependent localized surface plasmon resonances. Their unique optical property, high chemical stability, good biocompatibility, and easy functionalization make them promising candidates for a variety of biomedical applications, including bioimaging, biosensing, and cancer therapy. With the intention of enhancing their optical response in the near infrared window and endowing them with additional magnetic properties, Au nanoparticles have been integrated with other functional nanomaterials that possess complementary attributes, such as copper chalcogenides and magnetic metal oxides. The as constructed hybrid nanostructures are expected to exhibit unconventional properties compared to their separate building units, due to nanoscale interactions between materials with different physicochemical properties, thus broadening the application scope and enhancing the overall performance of the hybrid nanostructures. In this review, we summarize some recent progresses in the design and synthesis of noble metal Au-based hybrid inorganic nanostructures for nanomedicine applications, and the potential and challenges for their clinical translations.

Key words: Au nanoparticles; hybrid nanostructures; localized surface plasmon resonances; nanomedicine; theranostics

## Introduction

Although huge economic and scientific efforts have been invested in cancer research worldwide, more than 10 million new cancer cases are diagnosed each year, with death toll continues to rise [1-4]. Biomedical nanotechnology, including molecular diagnostic and nanotherapeutics that provide new options for clinical treatment, has recently been shown as a very promising technology to improve cancer patients' treatment outcomes and reduce the socioeconomic burden. Potential clinical applications of nanotechnology can be categorized depending on its usage on the body as either outside (such as "point-of-care" testing) or inside (such as diagnostics and targeted drug delivery). When focusing on their

clinical application inside the body, it is highly desirable to develop strategies that enable real-time tracking of the therapeutic response during the treatment, in order to avoid insufficient treatment or over-dosing side effect. In recent years, theranostic strategies based on various nanomaterials, noble metal Au nanoparticles (NPs) in particular, have received tremendous attention [5-14]. Under AC electromagnetic field (light), free charge carriers in Au NPs are driven into collective oscillations, displaying unique optical phenomena termed as localized surface plasmon resonance (LSPR). This intense light-matter interaction enables huge enhancement of local electromagnetic field, and has been widely

exploited in the fields of optical imaging, sensing, and photocatalysis [15-21]. Generally speaking, LSPR can be tuned over a wide spectral window from visible to the near infrared (NIR) region, depending on the NPs physicochemical properties such as size and morphology. Therefore, methods and protocols have been developed in different research labs for synthesizing Au NPs in a variety of shapes, such as nanosphere [22-24], nanocube [25], nanotriangle [26], nanocage [27], and nanoshell [28, 29]. By changing their size (1 to 100 nm), shape, and structure (single particle, alloy, heterodimer, core-shell, etc.), Au nanostructures can display unique linear and nonlinear optical behaviors, enabling their use as strong photosensitizers in phototherapy and *in vitro* diagnostics [27, 30-34]. Moreover, Au NPs possess large surface areas that can be conveniently functionalized with various biomolecules by means of Au-thiolate chemistry, facilitating the attachment of different moieties, such as antibodies, peptides, and biocompatible polymers with good biocompatibility and targeting capability [35, 36]. The development of facile synthesis and surface functionalization strategies of Au NPs have pushed forward their practical applications in the field of nano-biomedicine, including bioimaging [37-41], drug delivery [42-44], cancer diagnosis, and therapeutics [45-50].

Hybrid nanostructures composed of multiple domains with different compositions have attracted great interests in diverse research fields. For biomedical applications, hybrid nanostructures can provide multimodal imaging modality or imaging-therapy capability all-in-one single unit. More specifically, since Au possess excellent X-ray attenuation ability and high photothermal transduction efficiency, combining Au NPs with metal oxides or metal chalcogenides would either provide complementary imaging modality for accurate cancer diagnosis or offer additional therapeutic avenue for enhanced cancer treatment, thus overcoming the limitation of single theranostic model. Hence, the combined characteristics of Au-based nanostructures would be extremely valuable for their potential applications in precision nanomedicine. Moreover, the construction of plasmonic Au NPs based hybrid nanocomposites may effectively incorporate light absorption, magnetic response, and thermal effect in one single nanostructure. The mutual interaction between Au NPs and neighboring nanomaterials at the nanoscale contact can generate complex interfacial behaviors, such as electron transfer and near-field enhancement, which may induce changes in the effective carrier concentration and optical resonances [51-54]. This

plasmon-driven carrier density change and near-field effect in nanohybrids can lead to potential synergistic performance enhancement when compared to the simple sum of the isolated individual components. For example, it is demonstrated that Au NPs can activate the adjacent semiconductors or metal species, enabling increased photoenergy conversion or enhanced light-absorption properties, thus promoting reactive oxygen species (ROS) generation, photoacoustic signal amplification, and heat generation [55-57], benefiting the biomedical outcomes of photodynamic therapy (PDT), photoacoustic (PA) imaging, and photothermal therapy (PTT). Therefore, designing Au-based nanohybrids is a desirable strategy to achieve enhanced theranostic efficiency without increasing the dose of NPs applied, thus averting potential side effect [58-66]. These promising features together with their ease of surface modification make noble metal Au-based nanocomposites a powerful platform for diverse biomedical applications [67-73].

Some excellent reviews have summarized the advances of using noble metal NPs in the field of nanomedicine such as drug delivery, phototherapy, and biosensing [74-76]. However, reviews focusing specifically on Au NPs-based inorganic hybrid nanostructures for biomedical applications are still rare. In this review, we will focus on the design and synthesis of Au-based inorganic hybrid nanostructures, and their improved performance when being applied in the field of nanomedicine, such as bioimaging, cancer therapy, and drug delivery [77-81]. For the choice of adjoining components to Au, we limit our selection to copper chalcogenide, iron oxide, and manganese oxide, which are bioactive nanomaterials that can provide complementary theranostic potential to Au (as schematically illustrated in Figure 1). For each type of nanohybrid, a few important aspects will be discussed including the design and preparation of hybrid nanostructures, interaction between noble metal Au and the adjoining components, as well as their biomedical performance as theranostic agents (as briefed in Table 1).

## Au-Cu<sub>2-x</sub>E nanocomposites in nanomedicine

Other than the most researched noble metal nanocrystals, recent studies find that heavily-doped semiconductor nanocrystals such as non-stoichiometric copper chalcogenide NPs (Cu<sub>2-x</sub>E, where E = S, Se, Te; 0 < x ≤ 1) with different compositions can also support LSPR, due to their positively charged free carriers [82-86]. This opens up a new field for plasmonic research [87-94], as LSPR of semiconductor nanocrystals can be easily tuned from

visible to NIR by simply changing their doping levels. For biomedical applications, the emergence of copper chalcogenide nanocrystals circumvents the limitations experienced when using NIR absorbing anisotropic Au nanocrystals, which are generally large in size and unstable under laser irradiation conditions. Moreover, combining the traditional plasmonic noble metal Au with copper chalcogenide has attracted increasing attention in recent years. Many research groups have devoted efforts into constructing dual plasmonic noble metal-doped semiconductor nanocrystal hybrids, and investigated their coupled surface plasmon resonance properties and applications in the fields of catalysis and nanomedicine [77, 95, 96].

## Photothermal therapy

By changing the doping levels either chemically or electrochemically, the LSPR of  $\text{Cu}_{2-x}\text{E}$  can be tuned dynamically, showing characteristic LSPR peaks extendable to the second NIR (NIR-II) window (1000-1350 nm), which is the optimal biological transparent window with larger optical penetration depth and higher maximum permissible exposure of light irradiation over the traditional NIR-I window (700-950 nm) [97-101]. Through the construction of dual plasmonic nanohybrids, the LSPR coupling between Au and  $\text{Cu}_{2-x}\text{E}$  may open up a new regime for designing photo-absorbers with enhanced photothermal efficiency, an attractive attribute for imaging and therapy applications in the NIR-II window.

**Table 1.** Summary of Au-based inorganic hybrid nanostructures used in nanomedicine

Hybrid structure	Synthetic method	Size	Application	Advantage	Ref.
Au-Cu <sub>9</sub> S <sub>5</sub> UFO-shape	Seeded growth method	~22 nm (TEM)	PTT-CT	Improved heating effect	77
Au-Cu <sub>2-x</sub> Se heterodimer	Seeded growth method	~10 nm (TEM)	PA	Deep tissue imaging up to 17 mm	78
Au-Cu <sub>2-x</sub> S core-shell	Anion exchange	85.87±10 nm (DLS)	SERS/PA-PTT	Bimodal imaging-guided PTT	73
Au-Cu <sub>9</sub> S <sub>5</sub> @MSN	Seeded growth method	107 nm (DLS)	PTT-MRI	MRI tacking drug release	80
CuS@Cu <sub>2</sub> S@Au hollow structure	Template method	100 nm (TEM)	PTT-chemotherapy	Photo-switchable targeting	96
Au-Cu <sub>2-x</sub> S/Se core-shell or heterodimer	Seeded growth method	Tunable (TEM)	N.A	N.A	102
Au@Cu <sub>2-x</sub> S/Se core-shell	Self-assembly	Tunable (TEM)	PTT-PA-CT	High photothermal conversion efficiency	103
Cubic CuS@spiky Au core-shell	Template method	78±5 nm (DLS)	PTT-SERS	Enhanced PTT and SERS	109
Au-CuS yolk-shell structure	Template method and anion exchange	Tunable (TEM)	PTT-PDT-chemotherapy	Enhanced PTT and PDT	110
Au-Cu <sub>2-x</sub> S core-shell	Template method	150 nm (TEM)	Chemo-PTT	Enhanced photothermal effect	111
Fe <sub>3</sub> O <sub>4</sub> @Au core-shell	Seeded growth method	6.3 ± 0.7 nm (TEM)	Hyperthermia	Improved hyperthermia	121
Fe <sub>3</sub> O <sub>4</sub> /Au cluster/shell	Seeded growth method	240 nm (TEM)	SERS-magnetic hyperthermia	Improved hyperthermia	122
Fe@Au bi-layer semi-shell	Nanolithography and physical vapor deposition	40 nm (TEM)	CT, MRI and fluorescence	Magnetically amplified photothermal therapy	123
Fe <sub>3</sub> O <sub>4</sub> /Au cluster/shell	Seeded growth method	126±11 nm (TEM)	PTT-magnetic hyperthermia	Bimodal thermo-therapy	124
Au-Fe <sub>3</sub> O <sub>4</sub> heterodimer	Seeded growth method	11-14 nm (TEM)	MRI-CT	Bimodal imaging	136
Fe <sub>3</sub> O <sub>4</sub> @Au core-shell	One-pot hydrothermal	262.7±3.06 nm (DLS)	MRI-CT	Bimodal imaging	137
Fe <sub>2</sub> O <sub>3</sub> @Au core-shell	Seeded growth method	22.1±1.9 nm (TEM)	MRI-CT	Bimodal imaging	138
Fe <sub>3</sub> O <sub>4</sub> @SiO <sub>2</sub> @Au core-shell	Seeded growth method	222±1.5 nm (DLS)	MRI/CT(PA) imaging	Bimodal imaging	140
Fe <sub>2</sub> O <sub>3</sub> @Au core-shell	Seeded growth method	179 nm (DLS)	SERS-PA-MRI-PTT	Tri-modal imaging-guided PTT	141
Fe <sub>3</sub> O <sub>4</sub> @Au yolk-shell	Seeded growth method	65 nm (TEM)	MRI-PA-PET-chemo-thermal therapy	Multimodal imaging-guided chemo-thermal therapy	142
Fe <sub>3</sub> O <sub>4</sub> @Au@mSiO <sub>2</sub> core-shell	Seeded growth method	10.4 ± 2.3 nm (DLS)	PTT-PDT	Enhanced PDT	143
Au-Fe <sub>3</sub> O <sub>4</sub> heterodimer	Seeded growth method	16.7 ± 2.3 nm (TEM)	X-ray protection and X-ray enhancing agents	Discriminate healthy cell and cancer cell	144
MSN-Au-Fe <sub>3</sub> O <sub>4</sub> core-shell	Assembly	140 nm (TEM)	Nanozyme	Nanozyme-catalyzed cascade reaction	145
Au@mSiO <sub>2</sub> core-shell	Seeded growth method	50 nm (TEM)	Radiotherapy	Overcoming the hypoxia-associated radiotherapy resistance	158
Au cage@mSiO <sub>2</sub> core-shell	Seeded growth method	91 nm (TEM)	PDT	Boost immunogenic PDT	159
Cu <sub>2-x</sub> Se (Au)@MnO <sub>2</sub> core-shell	Seeded growth method	60 nm (TEM)	PTT	Redox-activated MRI-guided PTT	162
Au@mSiO <sub>2</sub> UFO-shaped	Seeded growth method	230 nm (TEM)	Dark field imaging	Monitoring cell membrane vesiculation	163
Au@mSiO <sub>2</sub> core-shell	Bio-templated method	20-25 nm (TEM)	Fluorometric and MRI based sensing	Inherent cross-validation	164

Abbreviations: PTT: photothermal therapy; PDT: photodynamic therapy; PA: photoacoustic imaging; CT: computed tomography; MRI: magnetic resonance imaging; SERS: surface enhanced Raman scattering; MSN: mesoporous silica nanoparticle; TEM: transmission electron microscopy; DLS: dynamic light scattering.

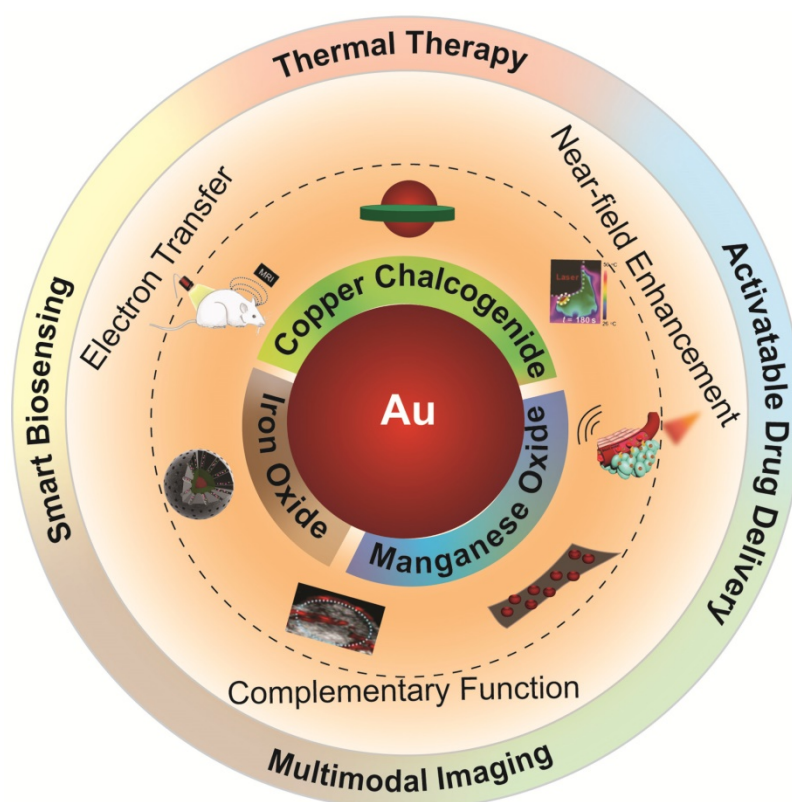


**Figure 1.** Illustration of various Au-based inorganic hybrid nanocomposites for diagnostic and therapeutic nanomedicine applications.

In 2014, our group constructed a dual plasmonic hybrid Au-Cu<sub>9</sub>S<sub>5</sub> with well-controlled interfaces [77]. Using the high purity heterodimer nanohybrid, we investigated the LSPR coupling effect originating from the collective electron and hole oscillations in the hybrid system, and found that the synergistic interactions between two components contributed to their enhanced photothermal performance in the NIR-II window. When comparing the molar extinction coefficient of the hybrid NP to that of its individual components (Au and Cu<sub>9</sub>S<sub>5</sub>), the Au-Cu<sub>9</sub>S<sub>5</sub> hybrid showed a 50% enhanced absorption at 1064 nm compared to pure Cu<sub>9</sub>S<sub>5</sub> NPs synthesized using the same protocol (Figure 2A). This enhanced NIR absorption further translated to improved heating capability (Figure 2B), as shown clearly in the thermal images (Figure 2C). The light penetration depth in the NIR-II window was also explored and a decay length of 5.3 mm at 1064 nm was determined. The experimentally measured photothermal performance and theoretical calculations revealed strong LSPR interaction between Au and Cu<sub>9</sub>S<sub>5</sub> domains in the nanohybrids. When being used for *in vivo* photothermal therapy, more than 10 °C increase was observed at tumor site under 1064 nm laser irradiation at a power density of 0.6 W cm<sup>-2</sup>, which is higher than the required effective temperature for cancer photothermal therapy (42-45 °C), thus inducing

significant tumor ablation (Figure 2D). By combining X-ray computed tomography (CT) imaging and photothermal therapy capabilities in one nanostructure, the Au-Cu<sub>9</sub>S<sub>5</sub> nanohybrids were demonstrated to be an attractive multifunctional platform for theranostic application. As the first report on efficient photothermal therapy in the NIR-II windows with power density lower than laser safety standards (1 W cm<sup>-2</sup>, ANSI Z136.1-2007, American National Standard for Safe Use of Lasers), this work reveals that constructing dual plasmonic nanostructures and optimizing the coupling effect of LSPR in nanohybrids is an efficient strategy to design better-performing theranostic agent in the NIR-II window.

Following the work of Au-Cu<sub>9</sub>S<sub>5</sub> nanohybrids construction, various synthetic methods have been deployed to integrate Au in different shapes with copper chalcogenides to form dual plasmonic nanostructures of tunable geometries, in order to explore their LSPR coupling effect and enhanced photothermal capacity. To establish a more general strategy for synthesizing dual plasmonic nanocomposites, our group developed a facile aqueous phase synthesis route to integrate plasmonic Au with self-doped semiconductor Cu<sub>2-x</sub>Se [102]. Using a Se-mediated approach, Au-Cu<sub>2-x</sub>Se hybrid nanocrystals with different Au core morphologies such as

nanoparticle, nanorod, and nanotriangle can be facilely synthesized. Moreover, Au-Cu<sub>2-x</sub>Se hybrid nanocrystals with different morphologies such as core-shell and heterodimer geometry can be obtained by varying the polymers used for nanocrystal stabilization. Independently, Xia and coworkers developed a general and eco-friendly method to synthesize core@shell Au@Cu<sub>2-x</sub>E (E = S, Se) dual plasmonic nanohybrids in aqueous solution for multimodal imaging and tumor therapy applications [103]. Due to the plasmonic coupling between noble metal core and semiconductor nanoshell, the as-prepared hybrid Au@Cu<sub>2-x</sub>S showed an extremely large extinction coefficient of 9.32 L g<sup>-1</sup> cm<sup>-1</sup> at 808 nm. Another approach for obtaining Au@Cu<sub>2-x</sub>S core@shell NPs with independently tunable core and shell morphology was developed by Zhang *et al.*, through a cation exchange enabled non-epitaxial strategy [95], where the nonstoichiometric

composition and thickness of the Cu<sub>2-x</sub>S shell can be precisely controlled.

### Photoacoustic imaging

Photoacoustic (PA) imaging modality is based on measuring the acoustic waves generated in biological tissues after short laser pulses excitation [104-106]. By combining the advantage of high spatial resolution from optical imaging and large penetration depth from ultrasound detection, PA imaging has become a fast-developing imaging technique with great potential in biomedical and clinical applications [41]. PA imaging contrast depends on the optical cross sections of the tissue and the injected imaging agents. Therefore, strongly absorbing plasmonic nanocrystals including Au and copper chalcogenides have been selected as candidates for PA imaging contrast enhancing agents [107-109].

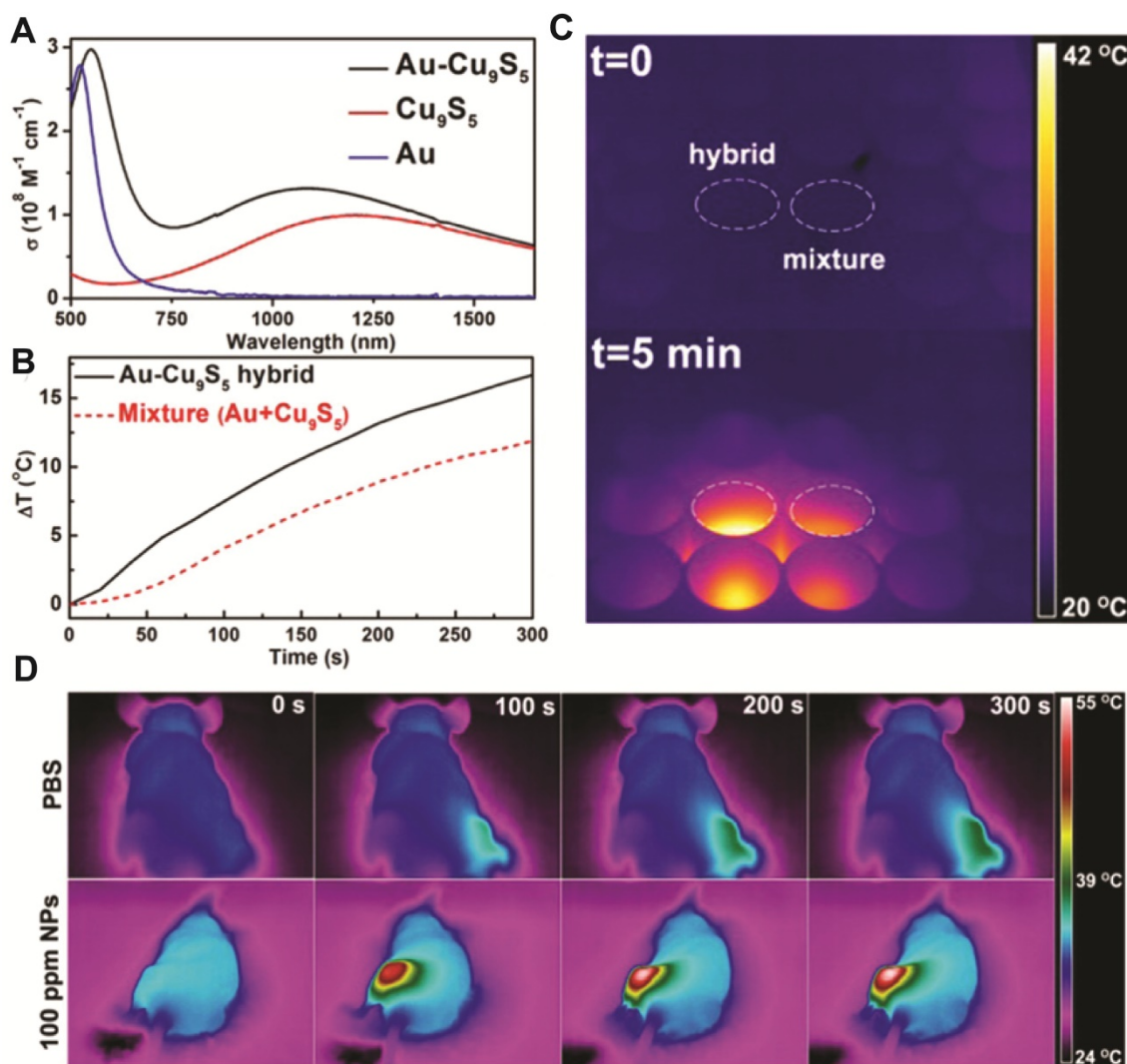


**Figure 2.** (A) Molar extinction coefficient of Au-Cu<sub>9</sub>S<sub>5</sub> hybrid nanostructures and corresponding Au and Cu<sub>9</sub>S<sub>5</sub> NPs. (B) Temperature increment of Au-Cu<sub>9</sub>S<sub>5</sub> hybrid nanostructures compared to the physical mixture of Au and Cu<sub>9</sub>S<sub>5</sub> NPs at the same concentrations. (C) Comparison of temperature changes captured by a thermal imaging camera from Au-Cu<sub>9</sub>S<sub>5</sub> hybrids and the physical mixture of Au and Cu<sub>9</sub>S<sub>5</sub> NPs under laser irradiation. (D) Representative thermal images of tumor-bearing mice under the irradiation of 1064 nm laser (0.6 W cm<sup>-2</sup>). Images are reproduced with permission from [77], copyright 2014 American Chemical Society.

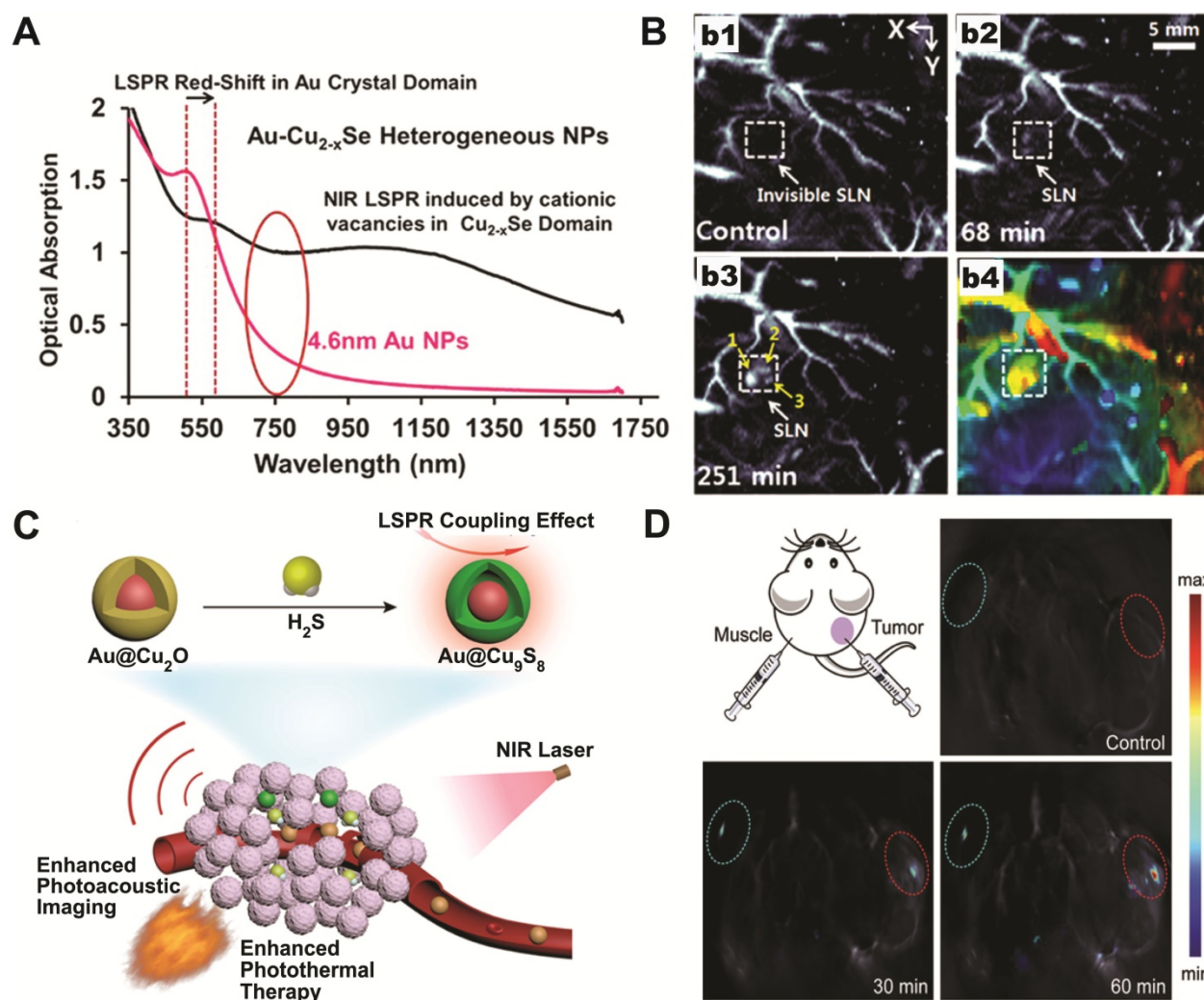


**Figure 3.** (A) UV-vis spectra of Au-Cu<sub>2-x</sub>Se heterodimers and the 4.6 nm Au seed NPs. (B) Representative PA imaging of sentinel lymph node before (b1) and after Au-Cu<sub>2-x</sub>Se injection for 68 min (b2) and 251 min (b3), and the depth-encoded PA coronal image (b4). Images are reproduced with permission from [78], copyright 2013 American Chemical Society. (C) Schematic illustration of endogenous H<sub>2</sub>S-triggered enhanced PA imaging and photothermal therapy based on LSPR coupling effect. (D) *In situ* sulfidation of Au@Cu<sub>2</sub>O nanocomposites and the corresponding PA images before and after intratumoral injection of Au@Cu<sub>2</sub>O nanostructures at different time points. Images are reproduced with permission from [81], copyright 2019 John Wiley and Sons.

Based on the plasmonic coupling induced enhanced photothermal response of Au-copper chalcogenides nanohybrids, Swihart and coworkers have reported using Au-Cu<sub>2-x</sub>Se heterodimer nanocrystals as contrast agents for deep tissue PA imaging [78]. The Au-Cu<sub>2-x</sub>Se heterodimer NPs exhibited a broad optical absorption spectrum across both NIR-I and NIR-II window, as a result of electron transfer between the constituting Au and Cu<sub>2-x</sub>Se domains (Figure 3A). Under 1064 nm excitation, with a power density (10 mJ cm<sup>-2</sup>) at only 1/10 of the ANSI safe limit, sentinel lymph node (SLN) mapping up to 17 mm under skin was achieved (Figure 3B), demonstrating their potential for clinical applications.

As photothermal and photoacoustic effects are intrinsically related to the light-matter interaction, the dual plasmonic Au-copper chalcogenides nanohybrids are perfect candidates for PA imaging-guided photothermal therapeutic applications operating at

the same NIR window. Nie *et al.* reported aqueous phase synthesis of Au@Cu<sub>2-x</sub>S core-shell NPs via anion exchange between S<sup>2-</sup> and Au@Cu<sub>2</sub>O core-shell NPs, which were then used for accurate tumor identification and efficient ablation through PA imaging-guided photothermal therapy (Figure 3C) [73]. The idea of chemical conversion from Cu<sub>2</sub>O to CuS using S<sup>2-</sup> was further utilized for smart theranostic agent design [81]. A characteristic physiological feature of colon cancer is the high level of endogenous hydrogen sulfide (H<sub>2</sub>S). Yang and coworkers have shown that the photothermal conversion efficiency of Au@Cu<sub>2</sub>O increased 50% in the presence of NaHS. Moreover, after intratumoral or intravenous injection, *in situ* sulfidation of Au@Cu<sub>2</sub>O by endogenous H<sub>2</sub>S in colon tumor was confirmed by both photoacoustic imaging (Figure 3D) and Raman spectroscopy. The converted Au@Cu<sub>9</sub>S<sub>8</sub> showed about twice stronger absorption at 808 nm, with increased

photothermal conversion efficiency  $\sim 1.2$  times higher than the original Au@Cu<sub>2</sub>O. This work demonstrates that the *in situ* generated Au-copper chalcogenides nanohybrids, formed by responding to local physiological niche environment at tumor site, can act as smart PA imaging-guided photothermal theranostic agent to treat cancers.

### Activatable drug delivery

Photothermal therapy can be used to eradicate tumor cells through localized heating. However, unsatisfactory tumor inhibition may occur due to inhomogeneous heating effect at tumor site. Combining chemotherapy with photothermal therapy has shown great promise in cancer treatment, where local heating can be used to regulate drug release with both spatial and dosage control, while the elevated local temperature also improves drug efficacy in treating cancer. To enable higher drug loading capacity, voids are often introduced into the nano-hybrid design. For instance, Lin *et al.* described the synthesis of hollow CuS@Cu<sub>2</sub>S@Au nanostructures, which not only exhibited enhanced photothermal conversion efficiency, but also afforded high drug loading capability by providing large cavity and mesoporous shell, thus enabling photo-responsive drug release under NIR laser excitation [96]. Zhang's group developed Au@void@CuS yolk-shell nanostructures as multifunctional drug carriers [110]. After doxorubicin (DOX) loading, the resultant DOX-Au-CuS yolk-shell nanocomposites could kill cancer cells more efficiently than the unloaded NPs under the same 980 nm laser irradiation conditions, due to the simultaneous photothermal and chemotherapeutic effect.

Drug delivery vehicles are often responding only to single stimulus such as external light irradiation or endogenous pH environment. Designing drug delivery system responding to multiple stimuli will not only minimize the undesirable release of chemotherapeutics thus avoiding adverse side effects, but also maximize the drug dosage in the target region with improved drug availability. To reach this goal, Cao *et al.* designed a dual responsive drug release system utilizing a rattle-type Au@Cu<sub>2-x</sub>S hollow mesoporous structure [111]. With this structure, a high drug loading capacity of 908  $\mu\text{g}$  DOX per mg of the hollow mesoporous nanocrystals was achieved. More importantly, the obtained hybrid nanostructures displayed both endogenous pH- and external photo-responsive drug release behaviors. The acidic pH mimicking tumor microenvironment and NIR laser irradiation could activate the drug delivery system with over 70% of DOX release in 20 min. This makes Au@Cu<sub>2-x</sub>S hollow mesoporous structure a

promising agent for chemo-photothermal therapy under photoacoustic imaging guidance, due to their superb photothermal conversion efficiency and conspicuous capability of photo activatable drug release property.

Further integrating activatable drug delivery system with real-time drug release monitoring function would enable patient-specific drug administration and benefit personalized medical treatment. Recently, based on the Au-Cu<sub>9</sub>S<sub>5</sub> nanostructures, we have developed a smart drug delivery platform with noninvasive activatable magnetic resonance (MR) imaging capacity for controllable drug release tracking [80]. The smart nanocomposites contained two functional components, which were the inner Au-Cu<sub>9</sub>S<sub>5</sub> core for heat generation under laser irradiation and outer mesoporous silica (MSN) shell for drug molecules loading and paramagnetic Gd<sup>3+</sup> ions anchoring (Figure 4A). The paramagnetic Gd<sup>3+</sup> ions-based chelates were used clinically to accelerate the longitudinal relaxation ( $T_1$ ) of excited protons, thus increasing the longitudinal relaxation rate ( $r_1$ ) and generating enhanced  $T_1$  MR images. Under exogenous NIR-II irradiation, localized heating of Au-Cu<sub>9</sub>S<sub>5</sub> core would melt the gatekeeper phase-change materials loaded in the MSN shell and trigger pulsated drug release with good on/off control (Figure 4B). With the released drug molecules leaving the hybrid nanocomposites, the accessibility of proton to the paramagnetic Gd<sup>3+</sup> ions anchored in the mesoporous channels was significantly promoted, which improved  $r_1$  of protons, and resulting in a positive correlation between  $T_1$  MR imaging signal and the amount of released drugs (Figure 4C), which was further verified at cellular (Figure 4D) and *in vivo* levels (Figure 4E).

### Au-Fe<sub>x</sub>O nanocomposites in nanomedicine

Iron oxide (Fe<sub>2</sub>O<sub>3</sub> and Fe<sub>3</sub>O<sub>4</sub>) with good chemical stability and biocompatibility has gained tremendous attention in diverse biomedical applications including magnetic resonance imaging, sensing, remote-controlled drug delivery, and magnetic hyperthermia [112-119]. By integrating magnetic iron oxide and plasmonic Au into one single unit, the as formed magneto-plasmonic hybrid nanostructures possess great potential in theranostic applications. Their optical and magnetic properties can be tuned independently by changing the respective nanoparticle domain size, shape, composition, and geometry. The unique attributes of magneto-plasmonic hybrid nanostructures have attracted great interests into their design and application for

simultaneous diagnosis and treatment of cancer.

### Thermal therapy

Thermal therapy is a promising approach to kill cancer cell with the local temperature at tumor site reaching 42-45 °C. Iron oxide and Au NPs are typical thermal agents that can generate heat to destroy tumor cells through noninvasive interaction with either oscillating magnetic field or NIR light [120]. However, both magnetic hyperthermia and photothermia have their inherent drawbacks. While noble metal Au-based photothermia show high heating efficiency with good spatial resolution, the compromised light penetration depth in living tissues set a limit on its potential clinical applications. On the

other hand, magnetic NP mediated hyperthermia employs radiofrequency, thus overcoming the penetration depth limitation of photothermia. Unfortunately, magnetic hyperthermia utilizing biocompatible iron oxide NPs suffers from their low specific loss powers. Extensive efforts have been put into modulating the size, magnetization or anisotropy of magnetic particles to enhance their specific absorption rate, thereby improving their heat generation capacity. Designing magneto-plasmonic nanostructures through hybridizing noble metal Au with magnetic nanomaterials together has been explored to overcome the limitations set by the individual components. It was found that by capping

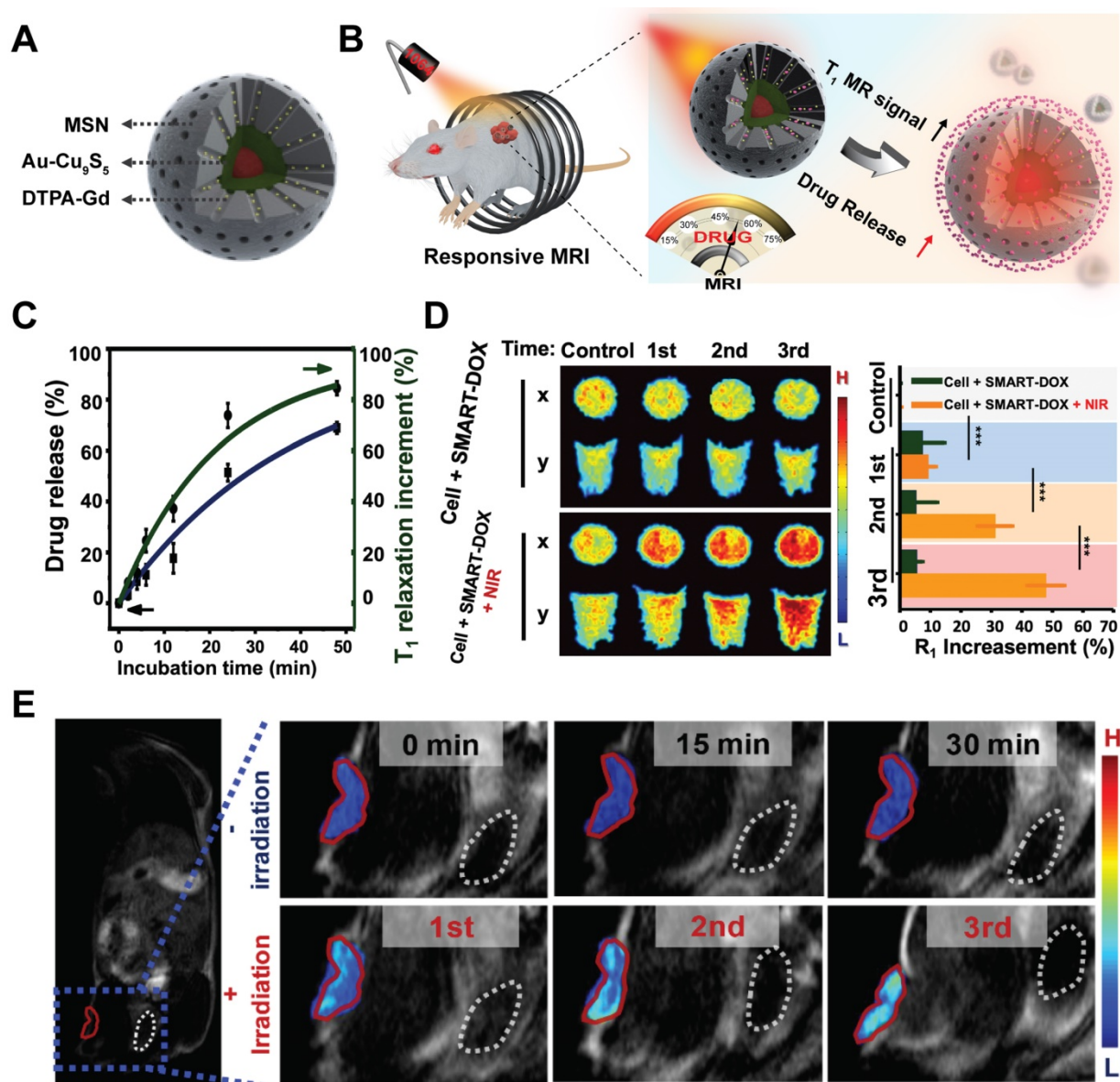


**Figure 4.** Schematic illustration of Au-Cu<sub>9</sub>S<sub>5</sub>@MSN nanostructures (A) and their NIR responsive drug release behavior with real time MRI monitoring property (B). (C) DOX release from Au-Cu<sub>9</sub>S<sub>5</sub>@MSN-DOX nanocomposites at 45 °C, and the corresponding T<sub>1</sub> relaxation increment. (D) Evolving T<sub>1</sub>-weighted MR images and MR relaxations of cancer cells treated with Au-Cu<sub>9</sub>S<sub>5</sub>-DOX nanocomposites after different repetition of NIR irradiations. (E) T<sub>1</sub>-weighted MR images of mice injected with Au-Cu<sub>9</sub>S<sub>5</sub>-DOX nanocomposites with and without laser irradiation treatments. Images are reproduced with permission from [80], copyright 2019 Springer Nature.

magnetic NPs with Au, more local heat could be generated when the hybrids were put under a radiofrequency field. Challa S. S. R. Kumar *et al.* demonstrated that superparamagnetic iron oxide ( $\text{Fe}_3\text{O}_4$ ) NPs (SPION, 5.4 nm) coated with 0.4-0.5 nm thick gold nanoshell can generate 4-5 times more heat compared to that of the pure  $\text{Fe}_3\text{O}_4$  NPs under a low-frequency oscillating magnetic field [121]. They speculated that the higher heat generation capacity was attributed to larger magnetic anisotropy of the superparamagnetic  $\text{Fe}_3\text{O}_4$  NPs inside Au shell. Zhou's group reported a similar study recently [122]. Under the same magnetic induction conditions, a local temperature of 15 °C higher was achieved with the hybrid  $\text{Fe}_3\text{O}_4/\text{Au}$  cluster/shell nanostructures compared to that of the pure  $\text{Fe}_3\text{O}_4$  NPs, and induced higher percentage of cancer cell apoptosis. Furthermore, the  $\text{Fe}_3\text{O}_4/\text{Au}$  nanostructures possessed high transverse relaxation rate ( $r_2$ ) for MR imaging (MRI), while the Au nanoshells can be used as surface enhanced Raman scattering (SERS) substrate for early diagnosis. SERS is a surface enhanced optical phenomenon, as Raman signals from surface-absorbed molecules are significantly amplified, due to the strongly enhanced near-field on the surface of noble metal NPs as the result of LSPR excitation. SERS allows optical sensing with high spatial resolution and sensitivity down to single molecule level under optimal conditions. Other than improving magnetic hyperthermia, photothermal effect can also be magnetically amplified via magnetophoretic manipulation strategy, as illustrate in the work by Sepúlveda *et al.* [123], where the optical heating efficiency of the Fe/Au nanodomains could be dramatically enhanced by local NPs enrichment in the laser irradiation zone under the assistance of an external magnetic field. In addition to single hyperthermia modality, magnetic hyperthermia and photothermia can be synergistically integrated in a properly designed magneto-plasmonic nanohybrid. Abou-Hassan and coworkers synthesized Au nanoshell coated iron oxide multi-core magneto-plasmonic nanohybrids with diameter of around 30 nm [124]. They demonstrated that the heat generated by the magneto-plasmonic nanohybrids display a cumulative effect when both magnetic and plasmonic heating modalities are working simultaneously. With the treatment dose only 1/10 of that used in typical magnetic hyperthermia therapy, a rapid temperature increase to 48 °C could be achieved in tumor tissue under simultaneous magnetic induction and laser irradiation treatment.

### Multimodal MR/(CT, PA, SERS) Imaging

Biomedical imaging is important for early

diagnosis and treatment evaluation, which has emerged as a key technology for the development of targeted therapies. Combining multiple imaging tools together can be very helpful in personal and precision medicine. While molecular imaging tools such as positron emission tomography (PET), computed tomography (CT), and FO (fluorescence optical) imaging have been widely used in clinical diagnostics, each of these imaging methods possesses its own strengths and weaknesses. In recent years, integrating different imaging modalities together by designing multimodal imaging agents such as CT/MR, FO/MR, PA/MR, and SERS/MR have been suggested to obtain more comprehensive pictures for accurate cancer diagnosis [125-132]. By integrating magnetic nanomaterials with Au, the concomitant MR imaging modality can provide non-invasive imaging, large penetration depth, and good soft tissue contrast.

Hybrid Au- $\text{Fe}_x\text{O}$  nanocomposites are considered potential bimodal CT/MR imaging agents [133-135], where  $\text{Fe}_x\text{O}$  component serves as  $T_1$  or  $T_2$  MR contrast enhancer, while Au with efficient X-ray attenuation capability works as powerful CT contrast enhancing agent. Gu *et al.* fabricated Au- $\text{Fe}_3\text{O}_4$  heterostructures for bimodal MR/CT imaging application by a seeded-growth method [136]. The prepared Au- $\text{Fe}_3\text{O}_4$  heterostructures were composed of 14 nm  $\text{Fe}_3\text{O}_4$  attached to 11 nm spherical Au NPs. The  $r_2$  value of the heterostructures was determined to be 136.4  $\text{mM}^{-1} \text{s}^{-1}$  at 1.5 T. Using a rabbit model, the Au- $\text{Fe}_3\text{O}_4$  heterostructure composites exhibited excellent MR/CT contrast enhancing performance. The rabbit liver can be clearly observed by MR imaging. Meanwhile, the detailed anatomical structures such as rabbit right ventricle can be clearly viewed by CT imaging. Using a facile one-pot strategy, Shi *et al.* reported core-shell  $\text{Fe}_3\text{O}_4@\text{Au}$  nanostructures for bimodal MR/CT imaging application [137]. The MR and CT performance evaluation showed that the hybrid NPs possess high  $r_2$  relaxivity (146.07  $\text{mM}^{-1} \text{s}^{-1}$ ) and excellent X-ray attenuation ability, which was then successfully applied to aorta CT imaging and liver MR imaging in mouse models. In another study, the same group fabricated  $\text{Fe}_3\text{O}_4/\text{Au}$  nanocomposites based on a layer-by-layer (LBL) strategy [135]. Their results demonstrated that at the optimized molar ratio of Au to  $\text{Fe}_3\text{O}_4$ ,  $\text{Fe}_3\text{O}_4/\text{Au}$  NPs exhibited excellent X-ray attenuation characteristics and a relatively high  $r_2$  relaxation rate of 92.67  $\text{mM}^{-1} \text{s}^{-1}$ . By further modifying them with targeting molecule folic acid, the hybrid nanocomposites could be specifically uptaken by cancer cells that over express folic acid receptors on cell membrane surface. Similarly, Zhang and Wang's group reported the use of lectin conjugated  $\text{Fe}_2\text{O}_3@\text{Au}$  as bimodal MR/CT imaging

agent *in vivo*, targeting specifically the colorectal cancer [138].

Besides attenuating X-rays for CT imaging, Au is also excellent PA imaging agent due to their LSPR characteristics. The construction of bimodal MR and PA molecular imaging agents can overcome the limitation of finite penetration depth of PA imaging, and provide structural and functional information of disease with high resolution and sensitivity. Melancon *et al.* fabricated multifunctional super-paramagnetic  $\text{Fe}_3\text{O}_4@Au$  nanoshells with excellent PA imaging performance and high  $r_2$  relaxivity of  $208 \text{ mM}^{-1} \text{ s}^{-1}$  [139]. Based on the high NIR absorption and strong magnetic properties of  $\text{Fe}_3\text{O}_4@Au$  nanoshells, the hybrid  $\text{Fe}_3\text{O}_4@Au$  nanoshells were capable of lighting up tumor region with PA-MR imaging. Moreover, the bimodal PA and MR imaging can be used to monitor the therapeutic treatment outcome mediated by the photothermal effect of  $\text{Fe}_3\text{O}_4@Au$ . Functionalizing  $Au\text{-Fe}_x\text{O}$  nanocomposites with targeting ligand could further improve their diagnostic capability. Franchini *et al.* synthesized a multilayered  $\text{Fe}_3\text{O}_4@SiO_2@Au$  core-shell nanostructure conjugated with folic acid [140]. With hydrodynamic diameter of  $222 \pm 1.5 \text{ nm}$ , the as-prepared nanostructure showed bimodal MR/PA imaging ability. After systemic injection into a tumor bearing mice, PA imaging revealed that  $\text{Fe}_3\text{O}_4@SiO_2@Au$  had exclusively accumulated in the ovarian cancer region after 4 h. These studies demonstrate the great potential of utilizing  $Au\text{-Fe}_x\text{O}$

hybrid nanostructures as bimodal MR/CT(PA) imaging agent for *in vivo* diagnostic applications. It is noteworthy that the biomedical imaging performance of hybrid nanostructures is strongly associated with their specific geometric arrangement. While both  $Au\text{-Fe}_3\text{O}_4$  heterostructure and  $\text{Fe}_3\text{O}_4@Au$  core-shell nanostructure can be used for bimodal MR/PA imaging, the core-shell  $\text{Fe}_3\text{O}_4@Au$  nanostructures with LSPR located in the NIR region are obviously more suitable for biomedical MR/PA imaging.

Zhang's group has investigated the potential of using  $Au\text{-Fe}_x\text{O}$  hybrid nanocomposites as multimodal SERS/PA/MR imaging-guided photothermal therapeutics by designing  $\text{Fe}_2\text{O}_3@Au$  core-shell structure (Figure 5A-B) [141]. The combined tri-modal imaging modality (SERS/PA/MR) can provide complementary information of anatomical tumor localization and tumor resection margin for accurate tumor diagnosis and surgical treatment guidance (Figure 5C-E). Furthermore, due to strong NIR absorbance derived from Au nanoshell,  $\text{Fe}_2\text{O}_3@Au$  core-shell nanostructures show high photothermal transduction efficiency for cancer therapy. The 4T1 tumor bearing mice administered with  $\text{Fe}_2\text{O}_3@Au$  core-shell nanostructures have shown significant photothermal tumor ablation under 808 nm laser irradiation. These results illustrated that rationally designed magneto-plasmonic hybrid nanostructures can be used for efficient multimodal imaging-guided photothermal cancer therapy.

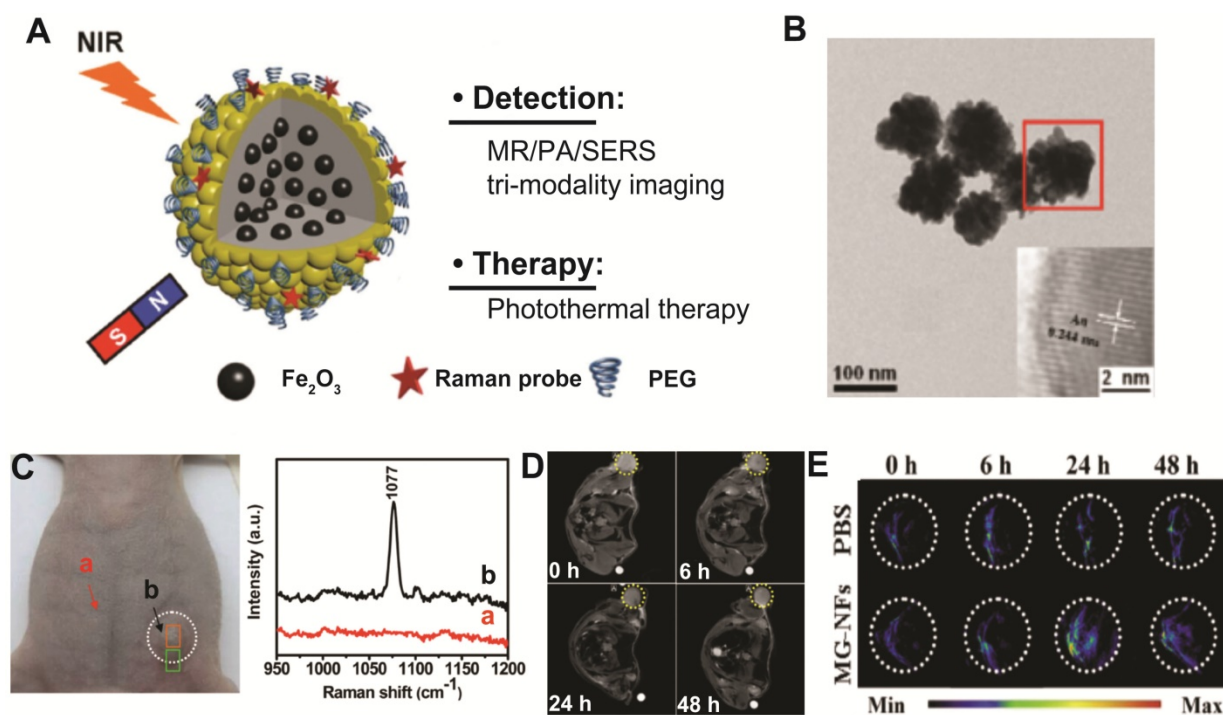


**Figure 5.** (A) Schematic illustration of  $\text{Fe}_2\text{O}_3@Au$  core-shell nanoflowers for multimodal imaging-guided tumor therapy. (B) Typical TEM image of  $\text{Fe}_2\text{O}_3@Au$  nanoflower structures. *In vivo* SERS spectra (C) from normal tissue (a) and tumor region (b),  $T_2$ -weighted MR images (D), and PA images (E) of a 4T1 tumor bearing mouse injected with either  $\text{Fe}_2\text{O}_3@Au$  nanoflowers or PBS. Images are reproduced with permission from [141], copyright 2015 John Wiley and Sons.

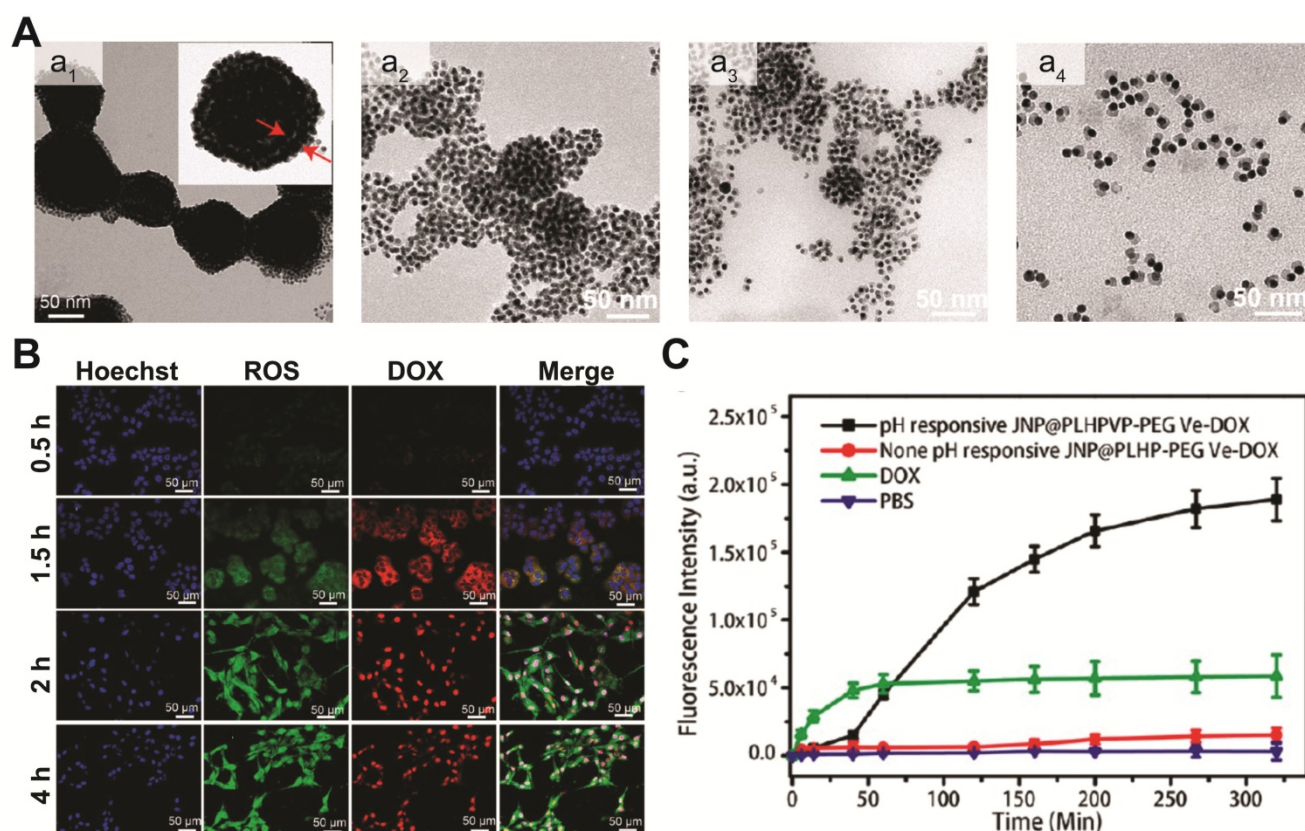


**Figure 6.** (A) Representative TEM images of assembled Fe<sub>3</sub>O<sub>4</sub>-Au janus structures (a<sub>1</sub>) after being incubated in acidic solution (pH=5.4) for 30 (a<sub>2</sub>), 60 (a<sub>3</sub>), and 90 min (a<sub>4</sub>). (B) Representative fluorescence images of tumor cells incubated with Fe<sub>3</sub>O<sub>4</sub>-Au-DOX nanocomposites at different time intervals. (C) Quantification of released DOX by measuring its fluorescence signals. Images are reproduced with permission from [79], copyright 2019 American Chemical Society.

### Activatable drug delivery

Under external stimulus such as NIR light and magnetic field, the multifunctional Au-Fe<sub>3</sub>O<sub>4</sub> hybrid nanostructures can not only act as *in vivo* diagnostic imaging agent, but also serve as powerful delivery vehicles for controlled drug release. In recent years, efforts have been put into developing different Au-Fe<sub>3</sub>O<sub>4</sub> hybrid nanostructures with high drug loading capacity, versatile targeting ability, and smart drug release capability. Chen and coworkers reported the synthesis of a yolk-shell plasmonic-magnetic hybrid theranostic platform [142], which was composed of a small Fe<sub>3</sub>O<sub>4</sub> core encapsulated inside a hollow cavity formed by a porous Au nanoshell. With a relative small size of around 65 nm, the yolk-shell Fe<sub>3</sub>O<sub>4</sub>-Au NPs displayed a high  $r_2$  value of 149.4 mM<sup>-1</sup> s<sup>-1</sup>, which is ~2.4 times of that from the core-shell structures, indicating that the interfacial interaction of the two components can greatly affect their magnetic properties. In addition, the hollow cavity can be an ideal storehouse for drug loading. After constructing a gatekeeper on the surface using thermosensitive poly(N-isopropylacrylamide-*co*-acrylamide), thermal responsive drug release is achieved under NIR light irradiation. Initially, only weak DOX fluorescence was

observed in the cells as a result of fluorescence quenching by Fe<sub>3</sub>O<sub>4</sub>-Au. Upon NIR exposure for 5 min, both cytoplasm and nucleus of the cells displayed strong red fluorescence, suggesting DOX was released, which was also confirmed in the *in vivo* study. In addition to light triggered drug delivery, pH responsive release system has also been widely adopted in different drug carrier designs. Recently, the same group developed a magnetic-plasmonic bilayer vesicle by assembling Fe<sub>3</sub>O<sub>4</sub>-Au janus structure with a pH-responsive polymer for multimodal imaging-guided cancer therapy [79]. The large hollow cavity formed in the assembled bilayer structures enables a high DOX loading capacity. Due to inter-particle plasmonic and magnetic coupling, the assembled bilayer structures displayed enhanced light absorption and high T<sub>2</sub> relaxivity, and exhibited improved MRI/PA contrast and photothermal activity, compared to the individual components. Moreover, the bilayer vesicles can be disassembled in mildly acidic microenvironment (Figure 6A). Therefore, DOX loaded in the hollow cavity can be released from the Fe<sub>3</sub>O<sub>4</sub>-Au-DOX bilayer vesicles, in response to the decreased pH level in tumor microenvironment (Figure 6B-C). Other than loading chemotherapy drugs, Au-Fe<sub>3</sub>O<sub>4</sub> hybrid

nanostructures can also carry singlet oxygen ( $^1\text{O}_2$ ) photosensitizers, and act as a potential agent for photodynamic therapy. For example, Rosa-Pardo *et al.* designed a core-shell  $\text{Fe}_3\text{O}_4@\text{Au}@m\text{SiO}_2$  nanostructure with photosensitizer Rose Bengal (RB) encapsulated inside mesoporous silica [143]. Due to the surface plasmon sensitization effect of Au shell, a 1.5-fold enhanced  $^1\text{O}_2$  generation by RB was detected. Furthermore, Au- $\text{Fe}_3\text{O}_4$  nanocomposites are also efficient ROS generating agents with their intrinsic enzyme-mimic characteristics [144-146]. By deliberately designing hybrid nanostructures with multi-enzymatic activities to achieve cascade reactions, high chemo-dynamic therapeutic efficiency has been demonstrated using inorganic nanohybrids. For example, Shi and Chen *et al.* constructed mesoporous silica coated Au- $\text{Fe}_3\text{O}_4$  nanostructures [145]. In tumor microenvironment, the Au domain behaves as glucose oxidase-mimicking nanozyme, catalyzing glucose to  $\text{H}_2\text{O}_2$  and gluconic acid. At the same time, the adjacent  $\text{Fe}_3\text{O}_4$  domain acts as peroxidase-mimicking nanozyme, reacting with the *in situ* generated  $\text{H}_2\text{O}_2$  and producing highly toxic ROS to kill cancer cells.

### Au-MnO<sub>2</sub> nanocomposites in nanomedicine

Besides iron oxides family, manganese oxides such as MnO,  $\text{MnO}_2$ , and  $\text{Mn}_3\text{O}_4$  have also been considered as promising candidates for biomedical applications [147-152]. As Mn is one of the essential trace elements in human body, Mn-based nanoparticles such as  $\text{MnO}_2$  can be utilized and metabolized by the human body. Mn-based complexes are considered as very promising clinical agents for  $T_1$  MR imaging. For instance, Mn-dipyridoxyl diphosphate (DPDP) complex Mangafodipir has already been approved as an efficient  $T_1$  MR agent for liver imaging. In addition,  $\text{MnO}_2$  nanomaterials can respond to tumor microenvironment cues such as hypoxia, acidosis, and vascular endothelial growth factor, which can be utilized to amplify their diagnostic and therapeutic performance. For example,  $\text{MnO}_2$  nanosheets will rapidly decompose and release  $\text{Mn}^{2+}$  under mildly acidic and reducing conditions, thus enhancing the contrast of  $T_1$  MR imaging [153, 153]. Moreover, the released  $\text{Mn}^{2+}$  could initiate Fenton chemistry to kill cancer cells by catalyzing tumor endogenous  $\text{H}_2\text{O}_2$  into toxic reactive oxygen species [149]. Therefore, combining  $\text{MnO}_2$  nanomaterials with the unique LSPR characteristics of noble metal Au can provide a promising theranostic platform as well as form smart probes for versatile biomedical applications both *in vitro* and *in vivo*.

### Enhanced radiotherapy/photodynamic therapy

Au- $\text{MnO}_2$ , a new kind of smart therapeutic agent, may serve as a potential theranostic candidate in the field of nanomedicine based on their good biocompatibility and tumor microenvironment responsive behaviors [149, 153-157]. The heavy atom Au can absorb X-rays to generate charged particles, and enhance the effect of radiotherapy (RT). Meanwhile, the  $\text{MnO}_2$  domain can react with endogenous  $\text{H}_2\text{O}_2$  in tumor microenvironment to generate oxygen locally, thus overcoming hypoxia-associated RT resistance. For this purpose, Liu *et al.* designed Au@ $\text{MnO}_2$  nanostructures [158], and they observed that Au@ $\text{MnO}_2$  hybrids indeed have enhanced radiotherapy efficiency as designed. In addition, the nanocomposites containing Au and  $\text{MnO}_2$  NPs also showed enhanced performance as photodynamic agents [159]. In treating metastatic triple-negative breast cancer, core-shell Au nanocage@ $\text{MnO}_2$  structures were able to boost immunogenic photodynamic therapy (PDT), thus inhibiting tumor growth and metastases. The enhanced therapeutic efficiency is attributed to the tumor microenvironment responsive oxygen generating  $\text{MnO}_2$  components, which was decomposed at acidic tumor  $\text{H}_2\text{O}_2$ -rich conditions and produced sufficient oxygen to boost PDT effect originating from the adjoining Au nanocage.

### Responsive imaging

Novel tumor microenvironment-responsive imaging agents have emerged as a promising class of theranostic agent for imaging-guided cancer treatment. By designing tumor microenvironment responsive nanoprobe, large off/on imaging contrast can be achieved. For example, Meng *et al.* prepared Au nanostar@ $\text{MnO}_2$  nanosheet hybrid structure of less than 50 nm in dimension [160]. With strong light absorption from 300 to 800 nm, the as synthesized hybrid can destroy tumor cells effectively through photothermal effect. Furthermore, the hybrid nanostructures displayed enhanced MR imaging capability in the presence of GSH, due to their redox environment responsive MR imaging capability. This study demonstrates the potential of Au- $\text{MnO}_2$  nanocomposites as efficient theranostic nanoprobe for activatable MR imaging-guided photothermal therapy. Other than photothermal therapy, many other therapeutic modalities such as photodynamic therapy and chemotherapy have also been integrated with  $\text{MnO}_2$  components. Lin's group designed  $\text{MnO}_2\text{-Pt}@Au_{25}$  nanocomposites, which combined photodynamic therapy, chemotherapy, and activatable MR imaging together in one system [161]. The  $\text{MnO}_2$  nanosheets acted as carrier for both

photosensitizer Au<sub>25</sub> and prodrug Pt(IV) loading. In the reducing tumor microenvironment, high level of GSH would be consumed through redox reaction with MnO<sub>2</sub> nanosheets and Pt(IV) prodrugs. As a result, both photodynamic therapeutic efficiency induced by Au<sub>25</sub> cluster and Pt(II) chemotherapy efficiency were enhanced. More importantly, the reduced Mn(II) ions released from MnO<sub>2</sub> nanosheets can increase the MR relaxivity from 401.9 mg<sup>-1</sup> s<sup>-1</sup> (r<sub>1</sub>) and 48.8 mg<sup>-1</sup> s<sup>-1</sup> (r<sub>2</sub>) to 471.3 mg<sup>-1</sup> s<sup>-1</sup> (r<sub>1</sub>) and 49.6 mg<sup>-1</sup> s<sup>-1</sup> (r<sub>2</sub>), thus enhancing their corresponding T<sub>1</sub> and T<sub>2</sub> MR imaging contrasts. Our group has also reported a feasible strategy to decorate various core materials including Au nanoparticle and Au nanorod with the tumor microenvironment-responsive MnO<sub>2</sub> shell, which can be utilized as activatable MRI-PTT theranostic platforms for cancer therapy [162].

### Smart biosensing platform

Under a dark-field microscope, a special condenser is used to block central light so that a circular light cone is incident on the object at high angle, only allowing oblique rays to hit the object. This blocks zeroth order light, and objects scatter light more strongly will stand out from the non-scattering dark background. Therefore, Au NPs with strong light-matter interaction due to their LSPR characteristics are perfect objects to be imaged under a dark-field microscope. In this regard, Au-MnO<sub>2</sub> nano hybrids are gaining interest as smart biosensors for probing complex cellular events. Xia and coworkers developed UFO-shaped Au-MnO<sub>2</sub> plasmonic supraparticles with diameter of around 230 nm, and used these anisotropic structures as dark-field contrast agents to probe the nano-bio interaction at the single cell level (Figure 7A-O) [163]. Due to the

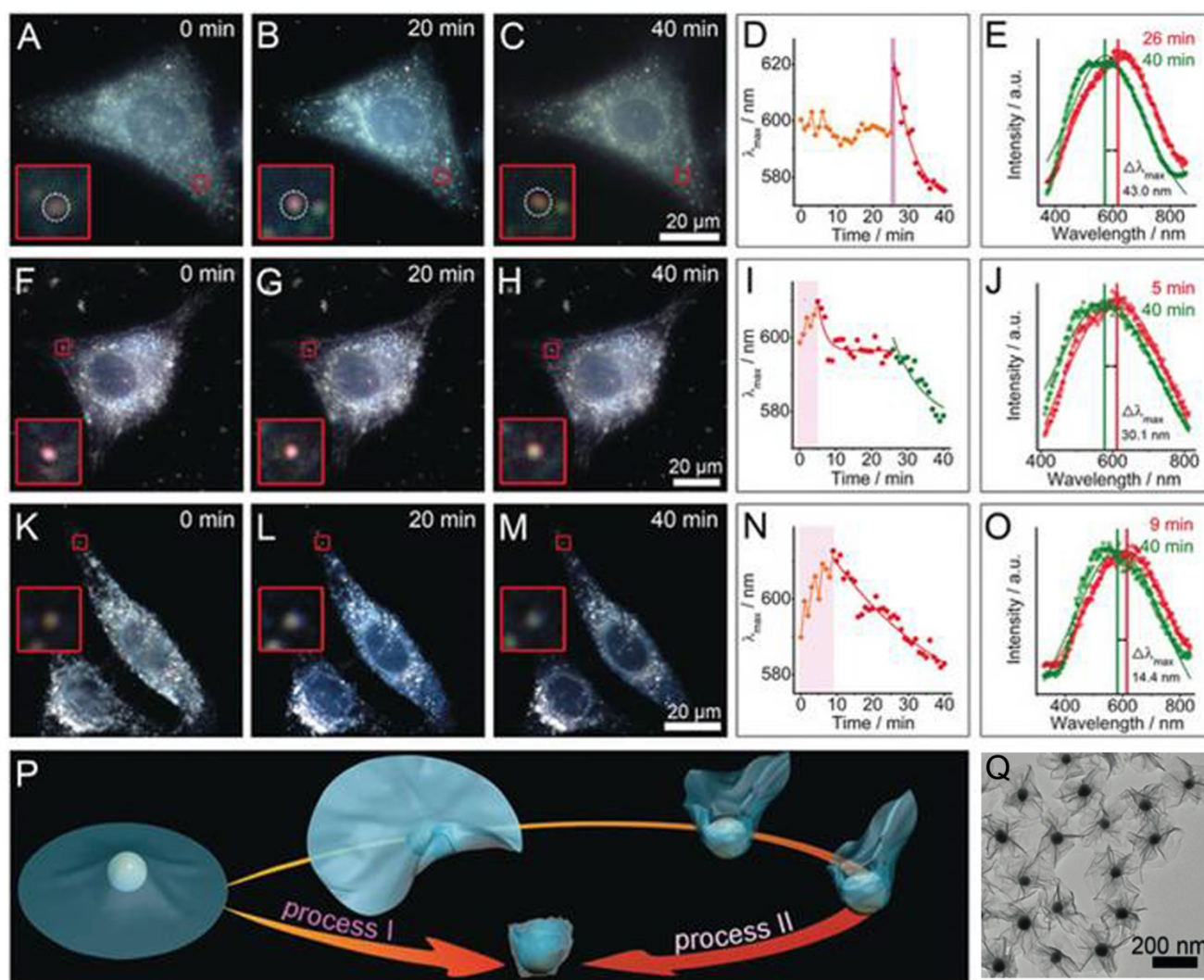


**Figure 7.** Interactions of the UFO-shaped 2D Au-MnO<sub>2</sub> nanostructures with different living cells probed by dark-field images and scattering spectra: (A-E) HepG2 cells, (F-J) 3T3 cells, and (K-O) buthionine sulfoximine (a GSH inhibitor) pre-treated HepG2 cells. (D, I, N) Time-dependent  $\lambda_{\max}$  of the scattering spectra changes (E, J, O) after entering the cells. (P) Schematic for two different types of transmembrane processes. (Q) TEM image of UFO-shaped 2D Au-MnO<sub>2</sub> nanostructures. Images reproduced with permission from [163], copyright 2019 John Wiley and Sons.

flexibility of thin  $\text{MnO}_2$  nanosheets, they can be physically deformed and folded during the endocytosis process. By employing dark-field spectroscopy, they visualized the interactions between 2D Au- $\text{MnO}_2$  nanostructures and living cells, and identified two definitely different trans-membrane processes (Figure 7P). During the cell membrane wrapping process, the deformation and folding of the thin  $\text{MnO}_2$  nanosheets (Figure 7Q) induced effective refractive index changes around Au NPs, rendering the NPs LSPR scattering red shift with different magnitudes depending on the endocytosis process. On the other hand, the presence of redox species within cells would disintegrate  $\text{MnO}_2$ , and induce a LSPR blue-shift, which could be employed to mark the complete cell membrane engulfment process. This LSPR modulation approach provides a convenient but efficient way to monitor the dynamic interactions between nanomaterials and cells. In addition to serve as a cellular probe, smart Au- $\text{MnO}_2$  nanocomposites can also be employed for point-of-care testing. Au@ $\text{MnO}_2$  hybrid nanocomposites have been developed to detect ascorbic acid (AA) in human serum [164]. The redox reaction between Au@ $\text{MnO}_2$  nanocomposites and AA resulted in the degradation of  $\text{MnO}_2$ , inducing both MR signal increase and fluorescence recovery due to free  $\text{Mn}^{2+}$  ions released from Au clusters. This Au- $\text{MnO}_2$  nanocomposite-based magnetic/fluorometric bimodal biosensor allows detection of AA in human serum with cross-validation.

### Other Au NPs-based nanocomposites

In addition to the above mentioned hybrid nanostructures, some other Au-based nanocomposites including Au-ZnO, Au- $\text{TiO}_2$ , and Au-reduced graphene oxide (rGO) have also been developed and utilized as new type of theranostic platforms for biomedical application [165-169]. Metal oxide NPs such as ZnO and  $\text{TiO}_2$  can absorb photons and create electron-hole pairs, generating ROS to inhibit microbial or cancer growth. However, they only absorb in the UV region, and their capability of ROS generation is limited by fast electron-hole recombination. By integrating ZnO or  $\text{TiO}_2$  with Au NPs, their optical absorption can be enhanced due to LSPR effect, the spectral window is extended to the visible, and the photo generated charge carrier recombination is greatly suppressed, leading to enhanced photocatalytic and PDT activity. For example, Yin *et al.* synthesized ZnO/Au hybrid nanostructures using a photo-reduction method [165]. It was found that even Au NPs of sizes less than 3 nm deposited on ZnO NPs can greatly enhance the photo-induced charge carriers in ZnO NPs and thus

promoting their ROS generation. Their result demonstrated that constructing hybrid nanostructures with Au is an efficient strategy to improve the photodynamic therapeutic effect of metal oxide. Au- $\text{TiO}_2$  NPs is another Au-based hybrid nanostructure with certain physicochemical properties outperforming their respective building blocks. For example, Yin *et al.* designed Au- $\text{TiO}_2$  nanostructures and explored their ROS generation capacity under ultrasound stimulation [166]. Their results revealed that the hybrid structures exhibited higher ROS generation efficiency and more significant tumor suppression effect than their counterparts without Au growth, demonstrating the potential of using Au- $\text{TiO}_2$  nanocomposite as sonosensitizer for cancer therapy. Another interesting Au NPs based-hybrid nanostructure is Au-rGO, as demonstrated by Lim *et al.*, where rGO was coated over Au nanorod [167, 168]. Due to high thermal conductivity of rGO and LSPR characteristic of Au nanorods, the prepared Au-rGO hybrid nanostructures exhibited amplified photothermal effect and PA signal intensity, compared to pure Au or graphene oxide/reduced graphene oxide. Moreover, Au can also be integrated with silica layer to form Au@silica nanostructure [169], thus combining the high drug loading capacity of silica with strong photothermal response of Au nanostructures, leading to better cancer cell killing outcome due to the synergistic effect of photothermia and NIR-induced drug release.

### Limitations and challenges

As reviewed briefly, many Au-based nanohybrids with enhanced physicochemical properties and bioactivities have been developed to date, which possess the potential to significantly improve cancer treatment outcomes. However, many challenges need to be resolved before they can be successfully translated to clinical usages.

### Synthetic challenges

Many synthetic issues remain to be addressed before we can explore the nanohybrids unique properties for nanomedicine. Although a rich library of noble metal Au-based nanocomposites is now available, their syntheses are generally complex with many reaction variables to tune. One critical question is how to establish a facile and general synthetic method that can build up the nanohybrids with the right functional building blocks of proper size, interface, and geometry [170]. Currently, the typical seeded growth route relies on depositing the second component on the seed NP nucleated *in situ* or synthesized in advance, which can be severely limited by the interfacial energy or lattice matching

requirements of the different crystalline domains. Moreover, the growth kinetics can be influenced by complicate synthetic conditions such as reaction temperature, concentration ratio of growth material to seeds NPs, and surface property of the seeds. Non-optimized procedures may lead to low yield of nanohybrids at the end of long tedious procedures. Therefore, developing general synthetic route and establishing standardized protocols to reliably prepare high-quality noble metal-based nanocomposites with controllable morphologies is highly desirable for their extensive biomedical applications.

### Biosafety

For clinical applications, the critical pharmacological behaviors such as biodistribution and biosafety of inorganic nanomaterials remain an under-explored territory. The physicochemical attributes such as NP size, shape, and surface coating are known to affect their cellular uptake, biodistribution, and nanotoxicity. This calls for systematic investigation on the *in vivo* behaviors of designed nanocomposites. The choice of chemical composition and surface coating is clearly critical for the nanocomposites biocompatibility. In terms of composition, Au NPs are generally considered to be bioinert, while copper chalcogenides and metal oxides may be etched or biodegraded in the body fluid, releasing metal ions and introducing potential toxicity to cells and organs. On the other hand, nanotoxicity is also strongly influenced by NP surface modifications. Surface coating can induce cytotoxicity effect directly or indirectly by influencing the formation of protein corona, and the subsequent cellular internalization and final fate of the NPs. As many of the NP physicochemical properties are highly interconnected, it is challenging to evaluate the cytotoxic effect originating from one single attribute of the NPs. Moreover, issues on the long-term metabolism of inorganic nanomaterials such as decomposition, degradation, and clearance of the nanocomposites from the body need to be addressed before they can be applied for clinical usage [171-177]. Although many cytotoxicity studies on Au NPs have suggested that they possess good biological safety within several weeks, a great risk of the bioinert NPs is that they may stay in the body and induce chronic toxicity over extended time. Therefore, a balanced stability, slow degradation, and fast clearance should be considered for nanohybrids design with proper choice of chemical composition and surface coating. Finally, the *in vitro/in vivo* models employed in the biosafety evaluation can also influence the behavior and fate of the hybrid NPs, which may render conflicting results.

To obtain accurate and consistent nanotoxicity evaluation, establishing standardized and reliable protocols to systematically investigate the impact of pharmacological parameters of the NPs is fundamentally important for the biosafety study of the hybrid NPs.

### Conclusions and perspectives

Nanohybrids composed of noble metal Au and copper chalcogenides or magnetic metal oxides have emerged as a unique class of material due to their interesting plasmon-magnetic properties, and the combined diagnostic and therapeutic functional units in one single entity. In this short review, we have summarized some recent developments in building up Au-based inorganic nanohybrids with controlled composition and structure, and highlighted progresses made in their theranostics applications.

Despite substantial progresses that have been made in the field of Au-based hybrid nanomedicine, this field is still at a rather preliminary stage from the standpoint of practical medical applications, especially in terms of biosafety that we have pointed out in the previous section. To address these important questions, several issues need to be addressed. First of all, more comprehensive studies need to be focused on the nanomaterial-biological system interactions, in order to better understand the critical factors determining the biosafety of nanocomposites, which will then be used for better nanomedicine design. Although plenty nanotoxicity studies have already been carried out on Au [36, 178-181], whether the attachment of a second component would affect its cellular behavior and final fate within organisms is still uncertain. It is believed that many physicochemical parameters of nanomaterials such as size, shape, charge, and surface modification can greatly influence the biocompatibility of nanocomposites. Future toxicity investigations on noble metal Au-based nanocomposites should consider all of these complex factors and explore the underlying molecular mechanisms of various factors on gene expression, signaling pathways, and downstream cell metabolism. In addition, when interpreting the interaction between nanocomposites and organism, it is necessary to note that the organisms may behave well and show normal physiological functions for a short period [182]. However, the organisms may suffer subtle but irreversible changes in their genetics after continuous exposure. Therefore, additional long-term toxicity evaluation is needed in the corresponding animal experiments. Moreover, excellent bioavailability and targeting ability is of great importance for highly efficient biomedical

nanotechnologies. The hybrid nanocomposites must avoid rapid clearance during blood circulation and increase their accumulation dosage at the desirable target site. Recently, the cell membrane-cloaking strategy by mimicking nanoparticles with erythrocyte or host cancer cell membrane envelopes has shown great potency in increasing circulation time by inhibiting macrophage recognition and improving targeting ability via homotypic binding [183-187]. However, this technique still faces some inherent challenges. For example, the detailed biomolecular mechanism of the homotypic binding derived from cell membrane is yet unclear. Identification of the specific ligands involved in the host membrane recognition would benefit future development of nanomaterial-based biomimetic nanotechnology. Furthermore, it is very difficult for the nanohybrids to go deep into solid tumors, which severely limits their efficacy as drug carrier and imaging platform. Knowledge on the NPs' pathway into tumors would be useful in helping design nanohybrids structures with improved tumor penetration depth. Despite the discovery of endothelial gaps in tumor vasculatures using developed animal models, nanomedicine design utilizing the enhanced permeability and retention (EPR) effect for human tumor treatment has been controversial. Only a few anticancer nanomedicines have received approval for clinical application based on EPR effect. Recently, new evidence has emerged, suggesting NPs may enter tumors via an active process through endothelial transcytosis [188]. These observations may establish new paradigms and enable novel strategies to help expedite the clinical translation of nanomedicine.

Au-based multifunctional nanocomposites have shown their promises in both early diagnostic and theranostic applications. Of note, their manifested multifunctionality due to the synergistic effect between different components would enable safer and more effective theranostic treatment. Undoubtedly, with continuing endeavor in the design and development of new multifunctional nanohybrids, it is our firm belief that they hold great diagnostic and therapeutic potential in broad biomedical applications, and are likely to find real significance in the new era of personalized precision nanomedicine.

## Acknowledgements

This work was funded by Six Talent Peaks Project in Jiangsu Province (SWYY-243) and National Natural Science Foundation of China (No. 21873113). X.G. Ding also acknowledges the start-up fund from Nanjing University of Posts and Telecommunications.

## Competing Interests

The authors have declared that no competing interest exists.

## References

- Naghavi M, Abajobir A, Abbafati C, Abbas K, Abd-Allah F, Abera S. GBD 2016 causes of death collaborators. global, regional, and national age-sex specific mortality for 264 causes of death, 1980-2016: a systematic analysis for the global burden of disease study 2016. *Lancet*. 2017; 390: 1151-1210.
- Bray F, Ferlay J, Soerjomataram I, Siegel R L, Torre L A, Jemal A. Global cancer statistics 2018: GLOBOCAN estimates of incidence and mortality worldwide for 36 cancers in 185 countries. *CA Cancer J Clin*. 2018; 68: 394-424.
- Torre LA, Trabert B, DeSantis CE, Miller KD, Samimi G, Runowicz CD, et al. Ovarian cancer statistics, 2018. *CA Cancer J Clin*. 2018; 68: 284-296.
- Zhang J, Jiang C, Longo JPF, Azevedo RB, Zhang H, Muehlmann LA. An updated overview on the development of new photosensitizers for anticancer photodynamic therapy. *Acta Pharm Sin B*. 2018; 8: 137-146.
- Zhang Z, Wang J, Chen C. Gold nanorods based platforms for light-mediated theranostics. *Theranostics*. 2013; 3: 223-238.
- Chen M, Tang S, Guo Z, Wang X, Mo S, Huang X, et al. Core-Shell Pd@Au Nanoplates as theranostic agents for in-vivo photoacoustic imaging, CT imaging, and photothermal therapy. *Adv Mater*. 2014; 26: 8210-8216.
- Zhang P, Hu C, Ran W, Meng J, Yin Q, Li Y. Recent progress in light-triggered nanotheranostics for cancer treatment. *Theranostics*. 2016; 6: 948-968.
- Liu Y, Yang X, Huang Z, Huang P, Zhang Y, Deng L, et al. Magneto-plasmonic janus vesicles for magnetic field-enhanced photoacoustic and magnetic resonance imaging of tumors. *Angew Chem Int Ed*. 2016; 55: 15297-15300.
- Jin J, Ovais M, Chen C. Stimulus-responsive gold nanotheranostic platforms for targeting the tumor microenvironment. *Nano Today*. 2018; 22: 83-99.
- Sun W, Luo L, Feng Y, Cai Y, Zhuang Y, Xie RJ, et al. Aggregation-induced emission gold clustoluminogens for enhanced low-dose X-ray-induced photodynamic therapy. *Angew Chem Int Ed*. 2020; 59: 9914-9921.
- Yang K, Liu Y, Wang Y, Ren Q, Guo H, Matson JB, et al. Enzyme-induced *in vivo* assembly of gold nanoparticles for imaging-guided synergistic chemo-photothermal therapy of tumor. *Biomaterials*. 2019; 223: 119460.
- Zhang Z, Yao Y, Yuan Q, Lu C, Zhang X, Yuan J, et al. Gold clusters prevent breast cancer bone metastasis by suppressing tumor-induced osteoclastogenesis. *Theranostics*. 2020; 10: 4042-4055.
- Ding Y, Sun Z, Tong Z, Zhang S, Min J, Xu Q, et al. Tumor microenvironment-responsive multifunctional peptide coated ultrasmall gold nanoparticles and their application in cancer radiotherapy. *Theranostics*. 2020; 10: 5195-5208.
- Ge X, Fu Q, Su L, Li Z, Zhang W, Chen T, et al. Light-activated gold nanorod vesicles with NIR-II fluorescence and photoacoustic imaging performances for cancer theranostics. *Theranostics*. 2020; 10: 4809-4821.
- Hu M, Chen J, Li ZY, Au L, Hartland GV, Li X, et al. Gold nanostructures: engineering their plasmonic properties for biomedical applications. *Chem Soc Rev*. 2006; 35: 1084-1094.
- Maier SA. *Plasmonics: fundamentals and applications*. Springer Science & Business Media. 2007.
- Anker JN, Hall WP, Lyandres O, Shah NC, Zhao J, Van Duyne RP. Biosensing with plasmonic nanosensors. In *Nanoscience and technology: a collection of reviews from nature journals*, World Scientific. 2010; p:308-319.
- Giannini V, Fernández-Domínguez AI, Heck SC, Maier SA. Plasmonic nanoantennas: fundamentals and their use in controlling the radiative properties of nanoemitters. *Chem Rev*. 2011; 111: 3888-3912.
- Qiu K, Du Y, Liu J, Guan JL, Chao H, Diao J. Super-resolution observation of lysosomal dynamics with fluorescent gold nanoparticles. *Theranostics*. 2020; 10: 6072-6081.
- Ye H, Liu Y, Zhan L, Liu Y, Qin Z. Signal amplification and quantification on lateral flow assays by laser excitation of plasmonic nanomaterials. *Theranostics*. 2020; 10: 4359-4373.
- Zhang A, Pan S, Zhang Y, Chang J, Cheng J, Huang Z, et al. Carbon-gold hybrid nanopores for real-time imaging, photothermal/photodynamic and nanozyme oxidative therapy. *Theranostics*. 2019; 9: 3443-3458.
- Boisselier E, Astruc D. Gold nanoparticles in nanomedicine: preparations, imaging, diagnostics, therapies and toxicity. *Chem Soc Rev*. 2009; 38: 1759-1782.
- Zhang XF, Liu ZG, Shen W, Gurunathan S. Silver nanoparticles: synthesis, characterization, properties, applications, and therapeutic approaches. *Int J Mol Sci*. 2016; 17: 1534.
- Carabineiro SAC. Applications of gold nanoparticles in nanomedicine: Recent advances in vaccines. *Molecules*. 2017; 22: 857.
- Skrabalak SE, Au L, Li X, Xia Y. Facile synthesis of Ag nanocubes and Au nanocages. *Nat Protoc*. 2007; 2: 2182-2190.
- Millstone JE, Hurst SJ, Métraux GS, Cutler JI, Mirkin CA. Colloidal gold and silver triangular nanoprisms. *Small*. 2009; 5: 646-664.
- Xia Y, Li W, Cobley CM, Chen J, Xia X, Zhang Q, et al. Gold nanocages: from synthesis to theranostic applications. *Acc Chem Res*. 2011; 44: 914-924.

28. Hirsch LR, Stafford RJ, Bankson JA, Sershen SR, Rivera B, Price R, et al. Nanoshell-mediated near-infrared thermal therapy of tumors under magnetic resonance guidance. *P Natl Acad Sci USA*. 2003; 100: 13549-13554.
29. Loo C, Lowery A, Halas N, West J, Drezek R. Immunotargeted nanoshells for integrated cancer imaging and therapy. *Nano Lett*. 2005; 5: 709-711.
30. Kinnear C, Moore TL, Rodriguez-Lorenzo L, Rothen-Rutishauser B, Petri-Fink A. Form follows function: nanoparticle shape and its implications for nanomedicine. *Chem Rev*. 2017; 117: 11476-11521.
31. Jain PK, Huang X, El-Sayed IH, El-Sayed MA. Noble metals on the nanoscale: optical and photothermal properties and some applications in imaging, sensing, biology, and medicine. *Acc Chem Res*. 2008; 41: 1578-1586.
32. Jain PK, El-Sayed MA. Plasmonic coupling in noble metal nanostructures. *Chem Phys Lett*. 2010; 487: 153-164.
33. Liu X, Zhang X, Zhu M, Lin G, Liu J, Zhou Z, et al. PEGylated Au@Pt nanodendrites as novel theranostic agents for computed tomography imaging and photothermal/radiation synergistic therapy. *ACS Appl Mater Interfaces*. 2017; 9: 279-285.
34. Deng Y, Tian X, Lu S, Xie M, Hu H, Zhang R, et al. Fabrication of multifoliate PtRu bimetallic nanocomplexes for computed tomography imaging and enhanced synergistic thermoradiotherapy. *ACS Appl Mater Interfaces*. 2018; 10: 31106-31113.
35. Soliman MG, Pelaz B, Parak WJ, Del Pino P. Phase transfer and polymer coating methods toward improving the stability of metallic nanoparticles for biological applications. *Chem Mater*. 2015; 27: 990-997.
36. Murphy CJ, Gole AM, Stone JW, Sisco PN, Alkilany AM, Goldsmith EC, et al. Gold nanoparticles in biology: beyond toxicity to cellular imaging. *Acc Chem Res*. 2008; 41: 1721-1730.
37. Dou Y, Guo Y, Li X, Li X, Wang S, Wang L, et al. Size-tuning ionization to optimize gold nanoparticles for simultaneous enhanced CT imaging and radiotherapy. *ACS Nano*. 2016; 10: 2536-2548.
38. Chhour P, Kim J, Benardo B, Tovar A, Mian S, Litt HI, et al. Effect of gold nanoparticle size and coating on labeling monocytes for CT tracking. *Bioconj Chem*. 2017; 28: 260-269.
39. Ashton JR, Castle KD, Qi Y, Kirscht DG, West JL, Badea CT. Dual-energy CT imaging of tumor liposome delivery after gold nanoparticle-augmented radiation therapy. *Theranostics*. 2018; 8: 1782-1797.
40. Yang X, Skrabalak SE, Li ZY, Xia Y, Wang LV. Photoacoustic tomography of a rat cerebral cortex *in vivo* with Au nanocages as an optical contrast agent. *Nano Lett*. 2007; 7: 3798-3802.
41. Fu Q, Zhu R, Song J, Yang H, Chen X. Photoacoustic imaging: contrast agents and their biomedical applications. *Adv Mater*. 2019; 31: 1805875.
42. Skrabalak SE, Au L, Lu X, Li X, Xia Y. Gold nanocages for cancer detection and treatment. *Nanomedicine*. 2007; 2: 657-668.
43. Sun T, Zhang YS, Pang B, Hyun DC, Yang M, Xia Y. Engineered nanoparticles for drug delivery in cancer therapy. *Angew Chem Int Ed*. 2014; 53: 12320-12364.
44. Yang M, Wang W, Qiu J, Bai MY, Xia Y. Direct visualization and semi-quantitative analysis of payload loading in the case of gold nanocages. *Angew Chem Int Ed*. 2019; 58: 17671-17674.
45. Song G, Cheng L, Chao Y, Yang K, Liu Z. Emerging nanotechnology and advanced materials for cancer radiation therapy. *Adv Mater*. 2017; 29: 1700996.
46. Espinosa A, Curcio A, Cabana S, Radtke G, Bugnet M, Kolosnjaj-Tabi J, et al. Intracellular biodegradation of Ag nanoparticles, storage in ferritin, and protection by a Au shell for enhanced photothermal therapy. *ACS Nano*. 2018; 12: 6523-6535.
47. Xi Z, Ye H, Xia X. Engineered noble-metal nanostructures for *in vitro* diagnostics. *Chem Mater*. 2018; 30: 8391-8414.
48. Xi Z, Cheng X, Gao Z, Wang M, Cai T, Muzzio M, et al. Strain effect in palladium nanostructures as nanozymes. *Nano Lett*. 2019; 20: 272-277.
49. Wang X, Qin L, Zhou M, Lou Z, Wei H. Nanozyme sensor arrays for detecting versatile analytes from small molecules to proteins and cells. *Anal Chem*. 2018; 90: 11696-11702.
50. Hu Y, Cheng H, Zhao X, Wu J, Muhammad F, Lin S, et al. Surface-enhanced Raman scattering active gold nanoparticles with enzyme-mimicking activities for measuring glucose and lactate in living tissues. *ACS Nano*. 2017; 11: 5558-5566.
51. Shaviv E, Schubert O, Alves-Santos M, Goldoni G, Di Felice R, Vallée F, et al. Absorption properties of metal-semiconductor hybrid nanoparticles. *ACS Nano*. 2011; 5: 4712-4719.
52. Khon E, Mereshchenko A, Tarnovsky AN, Acharya K, Klinkova A, Hewa-Kasakarage NN, et al. Suppression of the plasmon resonance in Au/CdS colloidal nanocomposites. *Nano Lett*. 2011; 11: 1792-9.
53. Zhang Z, Yates Jr JT. Band bending in semiconductors: chemical and physical consequences at surfaces and interfaces. *Chem Rev*. 2012; 112: 5520-5551.
54. Mokari T, Sztrum CG, Salant A, Rabani E, Banin U. Formation of asymmetric one-sided metal-tipped semiconductor nanocrystal dots and rods. *Nat Mater*. 2005; 4: 855-863.
55. Li Y, Wen T, Zhao R, Liu X, Ji T, Wang H, et al. Localized electric field of plasmonic nanoplatform enhanced photodynamic tumor Therapy. *ACS Nano*. 2014; 8: 11529-11542.
56. Song J, Yang X, Jacobson O, Lin L, Huang P, Niu G, et al. Sequential drug release and enhanced photothermal and photoacoustic effect of hybrid reduced graphene oxide-loaded ultrasmall gold nanorod vesicles for cancer therapy. *ACS Nano*. 2015; 9: 9199-9209.
57. Ji M, Xu M, Zhang W, Yang Z, Huang L, Liu J, et al. Structurally well-defined Au@Cu<sub>2</sub>S core-shell nanocrystals for improved cancer treatment based on enhanced photothermal efficiency. *Adv Mater*. 2016; 28: 3094-3101.
58. Park S, Lee WJ, Park S, Choi D, Kim S, Park N. Reversibly pH-responsive gold nanoparticles and their applications for photothermal cancer therapy. *Sci Rep*. 2019; 9: 20180.
59. Rossi A, Donati S, Fontana L, Porcaro F, Battocchio C, Proietti E, et al. Negatively charged gold nanoparticles as a dexamethasone carrier: stability in biological media and bioactivity assessment *in vitro*. *RSC Adv*. 2016; 6: 99016-99022.
60. Yang W, Liang H, Ma S, Wang D, Huang J. Gold nanoparticle based photothermal therapy: Development and application for effective cancer treatment. *Sustainable Mater Technol*. 2019; 22: e00109.
61. Porcaro F, Battocchio C, Antocchia A, Fratoddi I, Venditti I, Fracassi A, et al. Synthesis of functionalized gold nanoparticles capped with 3-mercaptopropylsulfonate and 1-thiogluco mixed thiols and *in vitro* biorespones. *Colloids Surf B*. 2016; 142: 408-416.
62. Grabowska-Jadach I, Kalinowska D, Drozd M, Pietrzak M. Synthesis, characterization and application of plasmonic hollow gold nanoshells in a photothermal therapy-new particles for theranostics. *Biomed Pharmacother*. 2019; 111: 1147-1155.
63. Fratoddi I, Venditti I, Battocchio C, Carlini L, Amatori S, Porchia M, et al. Highly hydrophilic gold nanoparticles as carrier for anticancer copper(I) complexes: loading and release studies for biomedical applications. *Nanomaterials*. 2019; 9: 772.
64. Khlebtsov N, Bogatyrev V, Dykman L, Khlebtsov B, Staroverov S, Shirokov A, et al. Analytical and theranostic applications of gold nanoparticles and multifunctional nanocomposites. *Theranostics*. 2013; 3: 167-80.
65. Venditti I. Engineered gold-based nanomaterials: morphologies and functionalities in biomedical applications. a mini review. *Bioengineering*. 2019; 6: 53.
66. Maccora D, Dini V, Battocchio C, Fratoddi I, Cartoni A, Rotili D, et al. Gold nanoparticles and nanorods in nuclear medicine: a mini review. *Applied Sciences*. 2019; 9: 3232.
67. Ma K, Li Y, Wang Z, Chen Y, Zhang X, Chen C, et al. Core-shell gold nanorod@layered double hydroxide nanomaterial with highly efficient photothermal conversion and its application in antibacterial and tumor therapy. *ACS Appl Mater Interfaces*. 2019; 11: 29630-29640.
68. Chen W, Zhang S, Yu Y, Zhang H, He Q. Structural-engineering rationales of gold nanoparticles for cancer theranostics. *Adv Mater*. 2016; 28: 8567-8585.
69. Ju Y, Zhang H, Yu J, Tong S, Tian N, Wang Z, et al. Monodisperse Au-Fe<sub>2</sub>C Janus nanoparticles: an attractive multifunctional material for triple-modal imaging-guided tumor photothermal therapy. *ACS Nano*. 2017; 11: 9239-9248.
70. Reguera J, de Aberasturi DJ, Henriksen-Lacey M, Langer J, Espinosa A, Szczupak B, et al. Janus plasmonic-magnetic gold-iron oxide nanoparticles as contrast agents for multimodal imaging. *Nanoscale*. 2017; 9: 9467-9480.
71. Kim D, Shin K, Kwon S G, Hyeon T. Synthesis and biomedical applications of multifunctional nanoparticles. *Adv Mater*. 2018; 30: 1802309.
72. Zeng J, Gong M, Wang D, Li M, Xu W, Li Z, et al. Direct synthesis of water-dispersible magnetic/plasmonic heteronanostructures for multimodal biomedical imaging. *Nano Lett*. 2019; 19: 3011-3018.
73. Lv Q, Min H, Duan DB, Fang W, Pan GM, Shen AG, et al. Total aqueous synthesis of Au@Cu<sub>2</sub>S core-shell nanoparticles for *in vitro* and *in vivo* SERS/PA imaging-guided photothermal cancer therapy. *Adv Healthc Mater*. 2019; 8: 1801257.
74. Jauffred L, Samadi A, Klingberg H, Bendix PM, Oddershede LB. Plasmonic heating of nanostructures. *Chem Rev*. 2019; 119: 8087-8130.
75. Lee SE, Lee LP. Biomolecular plasmonics for quantitative biology and nanomedicine. *Curr Opin Biotechnol*. 2010; 21: 489-497.
76. Lim WQ, Gao Z. Plasmonic nanoparticles in biomedicine. *Nano Today*. 2016; 11: 168-188.
77. Ding X, Liow CH, Zhang M, Huang R, Li C, Shen H, et al. Surface plasmon resonance enhanced light absorption and photothermal therapy in the second near-infrared window. *J Am Chem Soc*. 2014; 136: 15684-15693.
78. Liu X, Lee C, Law WC, Zhu D, Liu M, Jeon M, et al. Au-Cu<sub>2</sub>Se heterodimer nanoparticles with broad localized surface plasmon resonance as contrast agents for deep tissue imaging. *Nano Lett*. 2013; 13: 4333-4339.
79. Song J, Lin L, Yang Z, Zhu R, Zhou Z, Li ZW, et al. Self-assembled responsive bilayered vesicles with adjustable oxidative stress for enhanced cancer imaging and therapy. *J Am Chem Soc*. 2019; 141: 8158-8170.
80. Ding X, Zhao H, Li C, Wang Q, Jiang J. All-in-one theranostic nanoplatform with controlled drug release and activated MRI tracking functions for synergistic NIR-II hyperthermia-chemotherapy of tumors. *Nano Res*. 2019; 12: 2971-2981.
81. Tao C, An L, Lin J, Tian Q, Yang S. Surface plasmon resonance-enhanced photoacoustic imaging and photothermal therapy of endogenous H<sub>2</sub>S-triggered Au@Cu<sub>2</sub>O. *Small*. 2019; 15: 1903473.
82. Zhao Y, Pan H, Lou Y, Qiu X, Zhu J, Burda C. Plasmonic Cu<sub>2</sub>S nanocrystals: optical and structural properties of copper-deficient copper (I) sulfides. *J Am Chem Soc*. 2009; 131: 4253-4261.
83. Luther JM, Jain PK, Ewers T, Alivisatos AP. Localized surface plasmon resonances arising from free carriers in doped quantum dots. *Nat Mater*. 2011; 10: 361-366.
84. Comin A, Manna L. New materials for tunable plasmonic colloidal nanocrystals. *Chem Soc Rev*. 2014; 43: 3957-3975.

85. Buonsanti R, Milliron DJ. Chemistry of doped colloidal nanocrystals. *Chem Mater.* 2013; 25: 1305-1317.
86. Agrawal A, Cho SH, Zandi O, Ghosh S, Johns RW, Milliron DJ. Localized surface plasmon resonance in semiconductor nanocrystals. *Chem Rev.* 2018; 118: 3121-3207.
87. Liu Z, Liu X, Du Y, Ren J, Qu X. Using plasmonic copper sulfide nanocrystals as smart light-driven sterilants. *ACS Nano.* 2015; 9: 10335-10346.
88. Yang W, Guo W, Le W, Lv G, Zhang F, Shi L, et al. Albumin-bioinspired Gd:CuS nanotheranostic agent for *in vivo* photoacoustic/magnetic resonance imaging-guided tumor-targeted photothermal therapy. *ACS Nano.* 2016; 10: 10245-10257.
89. Kumar A, Kim S, Nam JM. Plasmonically engineered nanoprobes for biomedical applications. *J Am Chem Soc.* 2016; 138: 14509-14525.
90. Kriegel I, Scotognella F, Manna L. Plasmonic doped semiconductor nanocrystals: Properties, fabrication, applications and perspectives. *Phys Rep.* 2017; 674: 1-52.
91. Shan B, Zhao Y, Li Y, Wang H, Chen R, Li M. High-quality dual-plasmonic Au@Cu<sub>2-x</sub>Se nanocrystals with precise Cu<sub>2-x</sub>Se domain size control and tunable optical properties in the second near-infrared biowindow. *Chem Mater.* 2019; 31: 9875-9886.
92. Ding X, Fu D, Kuang Y, Zou Y, Yang X, Feng L, et al. Seeded growth of Cu<sub>2-x</sub>Se nanocrystals and their size-dependent phototherapeutic effect. *ACS Appl Nano Mater.* 2018; 1: 3303-3311.
93. Ou W, Zou Y, Wang K, Gong W, Pei R, Chen L, et al. Active manipulation of NIR plasmonics: the case of Cu<sub>2-x</sub>Se through electrochemistry. *J Phys Chem Lett.* 2018; 9: 274-280.
94. Sun X, Zou Y, Jiang J. Surface plasmon resonances enhanced click chemistry through synergistic photothermal and hot electron effects. *Chem Commun.* 2019; 55: 4813-4816.
95. Ji M, Xu M, Zhang W, Yang Z, Huang L, Liu J, et al. Structurally well-defined Au@Cu<sub>2-x</sub>S core-shell nanocrystals for improved cancer treatment based on enhanced photothermal efficiency. *Adv Mater.* 2016; 28: 3094-3101.
96. Deng X, Li K, Cai X, Liu B, Wei Y, Deng K, et al. A Hollow-structured CuS@Cu<sub>2</sub>S@Au nanohybrid: synergistically enhanced photothermal efficiency and photoswitchable targeting effect for cancer theranostics. *Adv Mater.* 2017; 29: 1701266.
97. Bashkatov A, Genina E, Kochubey V, Tuchin V. Optical properties of human skin, subcutaneous and mucous tissues in the wavelength range from 400 to 2000 nm. *J Phys D: Appl Phys.* 2005; 38: 2543.
98. Hong G, Robinson JT, Zhang Y, Diao S, Antaris AL, Wang Q, et al. *In vivo* fluorescence imaging with Ag<sub>2</sub>S quantum dots in the second near-infrared region. *Angew Chem Int Ed.* 2012; 51: 9818-9821.
99. Smith AM, Mancini MC, Nie S. Bioimaging: second window for *in vivo* imaging. *Nat Nanotechnol.* 2009; 4: 710-711.
100. Welscher K, Liu Z, Sherlock SP, Robinson JT, Chen Z, Daranciang D, et al. A route to brightly fluorescent carbon nanotubes for near-infrared imaging in mice. *Nat Nanotechnol.* 2009; 4: 773-780.
101. Huang J, Xie C, Zhang X, Jiang Y, Li J, Fan Q, et al. Renal-clearable molecular semiconductor for second near-infrared fluorescence imaging of kidney dysfunction. *Angew Chem Int Ed.* 2019; 58: 15120-15127.
102. Zou Y, Sun C, Gong W, Yang X, Huang X, Yang T, et al. Morphology-controlled synthesis of hybrid nanocrystals via a selenium-mediated strategy with ligand shielding effect: the case of dual plasmonic Au-Cu<sub>2-x</sub>Se. *ACS Nano.* 2017; 11: 3776-3785.
103. Zhu H, Wang Y, Chen C, Ma M, Zeng J, Li S, et al. Monodisperse dual plasmonic Au@Cu<sub>2-x</sub>E (E = S, Se) core@ shell supraparticles: aqueous fabrication, multimodal imaging, and tumor therapy at *in vivo* level. *ACS Nano.* 2017; 11: 8273-8281.
104. Li W, Chen X. Gold nanoparticles for photoacoustic imaging. *Nanomedicine.* 2015; 10: 299-320.
105. Weber J, Beard PC, Bohndiek SE. Contrast agents for molecular photoacoustic imaging. *Nat Methods.* 2016; 13: 639-650.
106. Wang LV, Hu S. Photoacoustic tomography: *in vivo* imaging from organelles to organs. *Science.* 2012; 335: 1458-1462.
107. Nagarathinam M, Chen J, Vittal JJ. From self-assembled Cu (II) coordination polymer to shape-controlled CuS nanocrystals. *Cryst Growth Des.* 2009; 9: 2457-2463.
108. Gao D, Sheng Z, Liu Y, Hu D, Zhang J, Zhang X, et al. Protein-modified CuS nanotriangles: a potential multimodal nanopatform for *in vivo* tumor photoacoustic/magnetic resonance dual-modal imaging. *Adv Healthc Mater.* 2017; 6: 1601094.
109. Lv Q, Gao MY, Cheng ZH, Chen Q, Shen AG, Hu JM. Rational synthesis of hollow cubic CuS@Spiky Au core-shell nanoparticles for enhanced photothermal and SERS effects. *Chem Commun.* 2018; 54: 13399-13402.
110. Chang Y, Cheng Y, Feng Y, Jian H, Wang L, Ma X, et al. Resonance energy transfer-promoted photothermal and photodynamic performance of gold-copper sulfide yolk-shell nanoparticles for chemophototherapy of cancer. *Nano Lett.* 2018; 18: 886-897.
111. Cao Y, Li S, Chen C, Wang D, Wu T, Dong H, et al. Rattle-type Au@Cu<sub>2-x</sub>S hollow mesoporous nanocrystals with enhanced photothermal efficiency for intracellular oncogenic microRNA detection and chemo-photothermal therapy. *Biomaterials.* 2018; 158: 23-33.
112. LaConte L, Nitin N, Bao G. Magnetic nanoparticle probes. *Mater Today.* 2005; 8: 32-38.
113. Jiang J, Gu H, Shao H, Devlin E, Papaefthymiou G C, Ying JY. Bifunctional Fe<sub>3</sub>O<sub>4</sub>-Ag heterodimer nanoparticles for two-photon fluorescence imaging and magnetic manipulation. *Adv Mater.* 2008; 20: 4403-4407.
114. Shao H, Min C, Issadore D, Liang M, Yoon TJ, Weissleder R, et al. Magnetic nanoparticles and microNMR for diagnostic applications. *Theranostics.* 2012; 2: 55-65.
115. Hervault A, Thanh NTK. Magnetic nanoparticle-based therapeutic agents for thermo-chemotherapy treatment of cancer. *Nanoscale.* 2014; 6: 11553-11573.
116. Shin TH, Choi Y, Kim S, Cheon J. Recent advances in magnetic nanoparticle-based multi-modal imaging. *Chem Soc Rev.* 2015; 44: 4501-4516.
117. Chen Y, Ding X, Zhang Y, Natalia A, Sun X, Wang Z, et al. Design and synthesis of magnetic nanoparticles for biomedical diagnostics. *Quant Imag Med Surg.* 2018; 8: 957-970.
118. Wang X, Zhang C, Du J, Dong X, Jian S, Yan L, et al. Enhanced generation of non-oxygen dependent free radicals by schottky-type heterostructures of Au-Bi<sub>2</sub>S<sub>3</sub> nanoparticles via X-ray-induced catalytic reaction for radiosensitization. *ACS Nano.* 2019; 13: 5947-5958.
119. Yang Z, Ding X, Jiang J. Facile synthesis of magnetic-plasmonic nanocomposites as T<sub>1</sub> MRI contrast enhancing and photothermal therapeutic agents. *Nano Res.* 2016; 9: 787-799.
120. Deatsch AE, Evans BA. Heating efficiency in magnetic nanoparticle hyperthermia. *J Magn Magn Mater.* 2014; 354: 163-172.
121. Mohammad F, Balaji G, Weber A, Uppu RM, Kumar CS. Influence of gold nanoshell on hyperthermia of superparamagnetic iron oxide nanoparticles. *J Phys Chem C.* 2010; 114: 19194-19201.
122. Han Y, Lei SL, Lu JH, He Y, Chen ZW, Ren L, et al. Potential use of SERS-assisted theranostic strategy based on Fe<sub>3</sub>O<sub>4</sub>/Au cluster/shell nanocomposites for bio-detection, MRI, and magnetic hyperthermia. *Mat Sci Eng: C.* 2016; 64: 199-207.
123. Li Z, Aranda-Ramos A, Güell-Grau P, Tajada JL, Pou-Macayo L, Piedrafita SL, et al. Magnetically amplified photothermal therapies and multimodal imaging with magneto-plasmonic nanodomains. *Appl Mater Today.* 2018; 12: 430-440.
124. Espinosa A, Bugnet M, Radtke G, Neveu S, Botton GA, Wilhelm C, et al. Can magneto-plasmonic nanohybrids efficiently combine photothermia with magnetic hyperthermia? *Nanoscale.* 2015; 7: 18872-18877.
125. Tang L, Yang X, Dobrucki LW, Chaudhury I, Yin Q, Yao C, et al. Aptamer-functionalized, ultra-small, monodisperse silica nanoconjugates for targeted dual-modal imaging of lymph nodes with metastatic tumors. *Angew Chem Int Ed.* 2012; 51: 12721-12726.
126. Wong RM, Gilbert DA, Liu K, Louie A Y. Rapid size-controlled synthesis of dextran-coated, <sup>64</sup>Cu-doped iron oxide nanoparticles. *ACS Nano.* 2012; 6: 3461-3467.
127. Chen F, Ellison PA, Lewis CM, Hong H, Zhang Y, Shi S, et al. Chelator-free synthesis of a dual-modality PET/MRI agent. *Angew Chem Int Ed.* 2013; 52: 13319-13323.
128. Chen Q, Li K, Wen S, Liu H, Peng C, Cai H, et al. Targeted CT/MR dual mode imaging of tumors using multifunctional dendrimer-entrapped gold nanoparticles. *Biomaterials.* 2013; 34: 5200-5209.
129. Hu DH, Sheng ZH, Zhang PF, Yang DZ, Liu SH, Gong P, et al. Hybrid gold-gadolinium nanoclusters for tumor-targeted NIREF/CT/MRI triple-modal imaging *in vivo*. *Nanoscale.* 2013; 5: 1624-1628.
130. Wei Q, Chen Y, Ma X, Ji J, Qiao Y, Zhou B, et al. High-efficient clearable nanoparticles for multi-modal imaging and image-guided cancer therapy. *Adv Funct Mater.* 2018; 28: 1704634.
131. Chen Q, Wen J, Li H, Xu Y, Liu F, Sun S. Recent advances in different modal imaging-guided photothermal therapy. *Biomaterials.* 2016; 106: 144-166.
132. Liu H, Lin W, He L, Chen T. Radiosensitive core/satellite ternary heteronanostructure for multimodal imaging-guided synergistic cancer radiotherapy. *Biomaterials.* 2020; 226: 119545.
133. Narayanan S, Sathy BN, Mony U, Koyakutty M, Nair SV, Menon D. Biocompatible magnetite/gold nanohybrid contrast agents via green chemistry for MRI and CT bioimaging. *ACS Appl Mater Interfaces.* 2012; 4: 251-260.
134. Yang M, Cheng K, Qi S, Liu H, Jiang Y, Jiang H, et al. Affibody modified and radiolabeled gold-iron oxide hetero-nanostructures for tumor PET, optical and MR imaging. *Biomaterials.* 2013; 34: 2796-2806.
135. Cai H, Li K, Li J, Wen S, Chen Q, Shen M, et al. Dendrimer-assisted formation of Fe<sub>3</sub>O<sub>4</sub>/Au nanocomposite particles for targeted dual mode CT/MR imaging of tumors. *Small.* 2015; 11: 4584-4593.
136. Zhu J, Lu Y, Li Y, Jiang J, Cheng L, Liu Z, et al. Synthesis of Au-Fe<sub>3</sub>O<sub>4</sub> heterostructured nanoparticles for *in vivo* computed tomography and magnetic resonance dual mode imaging. *Nanoscale.* 2014; 6: 199-202.
137. Li J, Zheng L, Cai H, Sun W, Shen M, Zhang G, et al. Facile one-pot synthesis of Fe<sub>3</sub>O<sub>4</sub>@Au composite nanoparticles for dual-mode MR/CT imaging applications. *ACS Appl Mater Interfaces.* 2013; 5: 10357-10366.
138. He X, Liu F, Liu L, Duan T, Zhang H, Wang Z. Lectin-conjugated Fe<sub>2</sub>O<sub>3</sub>@Au core@shell nanoparticles as dual mode contrast agents for *in vivo* detection of tumor. *Mol Pharm.* 2014; 11: 738-745.
139. Zhou M, Singhana B, Liu Y, Huang Q, Mitcham T, Wallace MJ, et al. Photoacoustic-and magnetic resonance-guided photothermal therapy and tumor vasculature visualization using theranostic magnetic gold nanoshells. *J Biomed Nanotechnol.* 2015; 11: 1442-1450.
140. Monaco I, Arena F, Biffi S, Locatelli E, Bortot B, La Cava F, et al. Synthesis of lipophilic core-shell Fe<sub>3</sub>O<sub>4</sub>@SiO<sub>2</sub>@Au nanoparticles and polymeric entrapment into nanomicelles: a novel nanosystem for *in vivo* active targeting and

- magnetic resonance-photoacoustic dual imaging. *Bioconj Chem.* 2017; 28: 1382-1390.
141. Huang J, Guo M, Ke H, Zong C, Ren B, Liu G, et al. Rational design and synthesis of  $\gamma\text{Fe}_2\text{O}_3$ @Au magnetic gold nanoflowers for efficient cancer theranostics. *Adv Mater.* 2015; 27: 5049-5056.
142. Lin LS, Yang X, Zhou Z, Yang Z, Jacobson O, Liu Y, et al. Yolk-shell nanostructure: an ideal architecture to achieve harmonious integration of magnetic-plasmonic hybrid theranostic platform. *Adv Mater.* 2017; 29: 1606681.
143. Rosa-Pardo I, Roig-Pons M, Heredia A A, Usagre J, Ribera A, Galian R E, et al.  $\text{Fe}_3\text{O}_4$ @Au@mSiO<sub>2</sub> as an enhancing nanoplatform for Rose Bengal photodynamic activity. *Nanoscale.* 2017; 9: 10388-10396.
144. Klein S, Smuda M, Harreiss C, Menter C, Distel LVR, Kryschi C. Bifunctional Au- $\text{Fe}_3\text{O}_4$  nanoheterodimers acting as X-ray protector in healthy cells and as X-ray enhancer in tumor cells. *ACS Appl Mater Interfaces.* 2019; 11: 39613-39623.
145. Gao S, Lin H, Zhang H, Yao H, Chen Y, Shi J. Nanocatalytic Tumor therapy by biomimetic dual inorganic nanozyme-catalyzed cascade reaction. *Adv Sci.* 2019; 6: 1801733.
146. Wang M, Wang D, Chen Q, Li C, Li Z, Lin J. Recent advances in glucose-oxidase-based nanocomposites for tumor therapy. *Small.* 2019; 15: 1903895.
147. Schladt TD, Shukoor MI, Schneider K, Tahir MN, Natalio F, Ament I, et al. Au@MnO nanoflowers: hybrid nanocomposites for selective dual functionalization and imaging. *Angew Chem Int Ed.* 2010; 49: 3976-3980.
148. Song M, Liu T, Shi C, Zhang X, Chen X. Bioconjugated manganese dioxide nanoparticles enhance chemotherapy response by priming tumor-associated macrophages toward M1-like phenotype and attenuating tumor hypoxia. *ACS Nano.* 2016; 10: 633-647.
149. Lin LS, Song J, Song L, Ke K, Liu Y, Zhou Z, et al. Simultaneous fenton-like ion delivery and glutathione depletion by MnO<sub>2</sub>-based nanoagent to enhance chemodynamic therapy. *Angew Chem Int Ed.* 2018; 57: 4902-4906.
150. Liu J, Chen Q, Feng L, Liu Z. Nanomedicine for tumor microenvironment modulation and cancer treatment enhancement. *Nano Today.* 2018; 21: 55-73.
151. Chen Y, Cong H, Shen Y, Yu B. Biomedical application of manganese dioxide nanomaterials. *Nanotechnology.* 2020; 31: 202001.
152. Wu J, Williams GR, Niu S, Yang Y, Li Y, Zhang X, et al. Biomimetic bimetallic oxide nanotheranostics for multimodal imaging-guided combination therapy. *Theranostics.* 2020; 10: 841-855.
153. Fu C, Duan X, Cao M, Jiang S, Ban X, Guo N, et al. Targeted magnetic resonance imaging and modulation of hypoxia with multifunctional hyaluronic acid-MnO<sub>2</sub> nanoparticles in glioma. *Adv Healthc Mater.* 2019; 8: 1900047.
154. Wei R, Gong X, Lin H, Zhang K, Li A, Liu K, et al. Versatile octapod-shaped hollow porous manganese (II) oxide nanoplatform for real-time visualization of cargo delivery. *Nano Lett.* 2019; 19: 5394-5402.
155. Wu M, Hou P, Dong L, Cai L, Chen Z, Zhao M, et al. Manganese dioxide nanosheets: from preparation to biomedical applications. *Int J nanomed.* 2019; 14: 4781.
156. Liu Y, Gong CS, Lin L, Zhou Z, Liu Y, Yang Z, et al. Core-shell metal-organic frameworks with fluorescence switch to trigger an enhanced photodynamic therapy. *Theranostics.* 2019; 9: 2791-2799.
157. Ding B, Zheng P, Ma PA, Lin J. Manganese oxide nanomaterials: synthesis, properties, and theranostic applications. *Adv Mater.* 2020; 32: 1905823.
158. Yi X, Chen L, Zhong X, Gao R, Qian Y, Wu F, et al. Core-shell Au@MnO<sub>2</sub> nanoparticles for enhanced radiotherapy via improving the tumor oxygenation. *Nano Res.* 2016; 9: 3267-3278.
159. Liang R, Liu L, He H, Chen Z, Han Z, Luo Z, et al. Oxygen-boosted immunogenic photodynamic therapy with gold nanocages@manganese dioxide to inhibit tumor growth and metastases. *Biomaterials.* 2018; 177: 149-160.
160. Liu J, Cui H, Yan S, Jing X, Wang D, Meng L. Gold nanostars decorated MnO<sub>2</sub> nanosheets for magnetic resonance imaging and photothermal erosion of lung cancer cell. *Mater Today Commun.* 2018; 16: 97-104.
161. Bi H, Dai Y, Yang P, Xu J, Yang D, Gai S, et al. Glutathione and H<sub>2</sub>O<sub>2</sub> consumption promoted photodynamic and chemotherapy based on biodegradable MnO<sub>2</sub>-Pt@Au<sub>25</sub> nanosheets. *Chem Eng J.* 2019; 356: 543-553.
162. Fu D, Ding X, Wu J, Li C, Wang Q, Jiang J. Cationic polyelectrolyte mediated synthesis of MnO<sub>2</sub>-based core-shell structures as activatable MRI theranostic platform for tumor cell ablation. *Part Part Syst Char.* 2018; 35: 1800078.
163. Ling Y, Zhang D, Cui X, Wei M, Zhang T, Wang J, et al. Direct monitoring of cell membrane vesiculation with 2D AuNP@MnO<sub>2</sub> nanosheet supraparticles at the single-particle level. *Angew Chem Int Edit.* 2019; 131: 10652-10656.
164. Yu J, Yang W, Xing S, Wang J, Han H, Zhang P, et al. Blended gold/MnO<sub>2</sub>@BSA nanoparticles for fluorometric and magnetic resonance determination of ascorbic acid. *Microchim Acta.* 2019; 186: 89.
165. He W, Kim HK, Wamer WG, Melka D, Callahan JH, Yin JJ. Photogenerated charge carriers and reactive oxygen species in ZnO/Au hybrid nanostructures with enhanced photocatalytic and antibacterial activity. *J Am Chem Soc.* 2014; 136: 750-757.
166. Deepagan VG, You DG, Um W, Ko H, Kwon S, Choi KY, et al. Long-circulating Au-TiO<sub>2</sub> nanocomposite as a sonosensitizer for ROS-mediated eradication of cancer. *Nano Lett.* 2016; 16: 6257-6264.
167. Lim DK, Barhoumi A, Wylie R, Reznor G, Langer R, Kohane DS. Enhanced photothermal effect of plasmonic nanoparticles coated with reduced graphene oxide. *Nano Lett.* 2013; 13: 4075-4079.
168. Moon H, Kumar D, Kim H, Sim C, Chang JH, Kim JM, et al. Amplified photoacoustic performance and enhanced photothermal stability of reduced graphene oxide coated gold nanorods for sensitive photoacoustic imaging. *ACS Nano.* 2015; 9: 2711-2719.
169. Yang X, Liu X, Liu Z, Pu F, Ren J, Qu X. Near-infrared light-triggered, targeted drug delivery to cancer cells by aptamer gated nanovehicles. *Adv Mater.* 2012; 24: 2890-2895.
170. Ding X, Peng F, Zhou J, Gong W, Slaven G, Loh KP, et al. Defect engineered bioactive transition metals dichalcogenides quantum dots. *Nat Commun.* 2019; 10: 41.
171. Peng F, Setyawati MI, Tee J K, Ding X, Wang J, Nga ME, et al. Nanoparticles promote *in vivo* breast cancer cell intravasation and extravasation by inducing endothelial leakiness. *Nat Nanotechnol.* 2019; 14: 279-286.
172. Baptista PV. Cancer nanotechnology-prospects for cancer diagnostics and therapy. *Curr Cancer Ther Rev.* 2009; 5: 80-88.
173. Hassan S, Prakash G, Ozturk AB, Saghazadeh S, Sohail MF, Seo J, et al. Evolution and clinical translation of drug delivery nanomaterials. *Nano Today.* 2017; 15: 91-106.
174. Agrahari V, Agrahari V. Facilitating the translation of nanomedicines to a clinical product: challenges and opportunities. *Drug Discov Today.* 2018; 23: 974-991.
175. Coty JB, Vauthier C. Characterization of nanomedicines: a reflection on a field under construction needed for clinical translation success. *J Control Release.* 2018; 275: 254-268.
176. Ioannidis JP, Kim BY, Trounson A. How to design preclinical studies in nanomedicine and cell therapy to maximize the prospects of clinical translation. *Nat Biomed Eng.* 2018; 2: 797-809.
177. Witzigmann D, Hak S, van der Meel R. Translating nanomedicines: thinking beyond materials? A young investigator's reply to 'the novelty bubble'. *J Control Release.* 2018; 290: 138-140.
178. Goodman CM, McCusker CD, Yilmaz T, Rotello VM. Toxicity of gold nanoparticles functionalized with cationic and anionic side chains. *Bioconj Chem.* 2004; 15: 897-900.
179. Carnovale C, Bryant G, Shukla R, Bansal V. Size, shape and surface chemistry of nano-gold dictate its cellular interactions, uptake and toxicity. *Prog Mater Sci.* 2016; 83: 152-190.
180. Jia YP, Ma BY, Wei XW, Qian ZY. The *in vitro* and *in vivo* toxicity of gold nanoparticles. *Chin Chem Lett.* 2017; 28: 691-702.
181. Ginzburg AL, Truong L, Tanguay RL, Hutchison JE. Synergistic toxicity produced by mixtures of biocompatible gold nanoparticles and widely used surfactants. *ACS Nano.* 2018; 12: 5312-5322.
182. Conde J, Doria G, Baptista P. Noble metal nanoparticles applications in cancer. *J Drug Deliv.* 2012; 2012: 751075.
183. Fang RH, Hu CMJ, Luk BT, Gao W, Copp JA, Tai Y, et al. Cancer cell membrane-coated nanoparticles for anticancer vaccination and drug delivery. *Nano Lett.* 2014; 14: 2181-2188.
184. Wan Y, Wang L, Zhu C, Zheng Q, Wang G, Tong J, et al. Aptamer-conjugated extracellular nanovesicles for targeted drug delivery. *Cancer Res.* 2018; 78: 798-808.
185. Han X, Shen S, Fan Q, Chen G, Archibong E, Dotti G, et al. Red blood cell-derived nanoerythrocyte for antigen delivery with enhanced cancer immunotherapy. *Sci Adv.* 2019; 5: eaaw6870.
186. Jiang Y, Chekuri S, Fang RH, Zhang L. Engineering biological interactions on the nanoscale. *Curr Opin Biotechnol.* 2019; 58: 1-8.
187. Zhou J, Kroll AV, Holay M, Fang RH, Zhang L. Biomimetic nanotechnology toward personalized vaccines. *Adv Mater.* 2019; p:1901255.
188. Sindhvani S, Syed AM, Ngai J, Kingston BR, Maiorino L, Rothschild J, et al. The entry of nanoparticles into solid tumours. *Nat Mater.* 2020; 19: 566-575.